

Analysis of hydro-abrasive erosion in a high-head Pelton turbine injector using a Eulerian-Lagrangian approach

Proc IMechE Part A:
J Power and Energy
2023, Vol. 0(0) 1–20
© IMechE 2023
Article reuse guidelines:
sagepub.com/journals-permissions
DOI: 10.1177/09576509231218043
journals.sagepub.com/home/pia


Navam Shrivastava¹ , Anant Kumar Rai¹ , Ali Abbas²  and Yexiang Xiao³ 

Abstract

High-head hydropower plants deploy Pelton turbines to harness energy; however, turbine components face severe abrasive erosion due to suspended sediments. The erosion of the Pelton injector leads to the degradation of the jet quality, reducing the turbine efficiency considerably. Recently, the erosion of an internal servomotor design of the injector has been studied numerically; however, the cavitation-erosion synergy was not explored. This study serves as the extension of the literature with an analysis of the hydro-abrasive erosion and inception of cavitation in an injector with an external servomotor of a high-head hydropower plant (HPP). A Eulerian-Lagrangian approach is used to study the effects of sediment properties and flow parameters on hydro-abrasive erosion; whereas, the Schnerr-Sauer model is used to analyze the inception of cavitation. Interestingly, an increase in particle size from 40 microns to 200 microns resulted in a 95.7% reduction in needle erosion; but, led to a two-fold increase in nozzle erosion. For an increase in the plant head from 200 m to 820 m, the increase in erosion rate of the nozzle and the needle is 4.36 and 1.4 times, respectively. Moreover, the possibility of cavitation in the Pelton injector also increases with an increase in the head of the HPP leading the injector to higher susceptibility to the synergic effect of cavitation and hydro-abrasive erosion. This study attempts to assist the hydropower development in high-head regions with a risk of high sediment flow and manage the existing plants efficiently.

Keywords

Hydropower, abrasive erosion, particle-laden flow, Pelton injector, cavitation, eulerian-Lagrangian method

Date received: 19 June 2023; accepted: 15 November 2023

Introduction

Currently, most of the power generation utilizes the non-renewable source of energy, which is one of the main reasons for global warming and climate change. In 2021, the CO₂ level increased by 6% compared to the preceding year. It necessitates switching to more renewable-based sources for power generation where hydropower has the maximum contribution among all renewable-based sources. In 2021, 53.7% of the electricity generated globally from renewable-based sources came from hydropower.¹ Climate change has severe impacts on rainfall patterns resulting in soil erosion and retreating glaciers leading to high sediment flows in streams. These sediments pose a major challenge to renewable energy generation in the form of electricity as hydropower plant (HPP) is the highest contributor to renewable-based electricity. The two major challenges are the depletion of reservoir capacity and abrasive erosion of components of the waterways.² Though hydropower is of prime importance in the quest for clean energy with the highest conversion efficiency among all renewable energy sources, a large potential still remains unexploited due to the severe erosion of turbine components.³ Even the existing HPPs face issues of reduction in generation efficiency and frequent shut-downs due to abrasive erosion in run-of-river HPPs located in geologically young mountains like the

Himalayas, the Andes, and the Alps.^{4,5} One of the most used hydraulic machinery in high-head HPPs is a Pelton turbine designed for high-velocity flows to convert the majority of the available hydraulic energy. In the Pelton turbines, even particles smaller than 60 μm can cause severe damage to the turbine components like injectors and buckets due to high flow velocities.⁶ The erosion in Pelton turbine components is a complex process and has not been explored completely.

Hydro-abrasive erosion, a progressive and cumulative process, alters the profile of the turbine components affecting the flow conditions.^{7,8} This results in a progressive decline of turbine efficiency over a period of time and loss of generation. After conducting several tests, Padhy and Saini⁷ observed a 3.5% mass reduction of a model Pelton

¹Department of Mechanical Engineering, National Institute of Technology Warangal, Warangal, India

²Flovel Energy Private Limited, Faridabad, India

³State Key Laboratory of Hydrosience and Engineering & Department of Energy and Power Engineering, Tsinghua University, Beijing, China

Corresponding author:

Yexiang Xiao, State Key Laboratory of Hydrosience and Engineering & Department of Energy and Power Engineering, Tsinghua University, Beijing 100084, China.

Email: xiaoyex@mail.tsinghua.edu.cn

bucket due to hydro-abrasive erosion resulting in an 8% efficiency loss. In Chenani HPP, the nozzle and needle operating in an erosive environment underwent a 5% and 3.71% loss of volume at the end of 2712 h of operation.⁹ In general, a 1% increase in the splitter width of the Pelton bucket due to hydro-abrasive erosion results in a 1% drop in Pelton turbine efficiency.¹⁰ Hydro-abrasive erosion near the nozzle exit increases the nozzle opening area, increasing the jet diameter. Such increased jet diameter results in reducing the Pelton turbine efficiency as observed by Alomar et al.¹¹ Therefore, it becomes important to predict the erosion rate with an erosion model to estimate the efficiency reduction, sediment cut-off concentration, and time between overhauls.^{7,12,13} To develop a correlation between erosion rate and the different parameters involved, experiments were carried out using a rotating type test rig or a jet erosion tester.¹⁴ However, the test rigs do not completely replicate the erosive conditions of Pelton turbine components mainly due to high heads and dilute sediment conditions in actual HPPs.^{7,15,16} The Data-driven approach can also be utilized in predicting and monitoring the erosion rate in the Pelton turbine, optimizing maintenance cost.¹⁷ Usually, the operating heads within 200 m were tested in model Pelton turbines^{7,15,16}; whereas, high-head turbines often have designed heads in the range of 800–1300 m. Thus, the application of erosion models developed experimentally considering sediment parameters like size, concentration, shape and hardness, turbine material, and head of the HPP have limited applications in Pelton turbines. The erosion rate and failure mechanism are mainly obtained from analysis of the eroded components of the turbines, especially for high-head HPPs.^{9,18,19}

Several studies reported efficiency loss in HPP due to hydro-abrasive erosion in the range of 4%–15% for a short period of 3–4 months.^{19–21} In the field study by Dufour at the Klosterli HPP (1 × 2.6 MW) located in the Alps mountains, the maximum efficiency loss reached 8% within 105 days.²¹ In another study of turbine erosion in the Alps mountains, Felix²² observed a reduction of 0.9% in turbine efficiency of Fieschertal HPP (2 × 32 MW) located in the Alps mountains due to hydro-abrasive erosion for the 1902 h of operation period. In the Himalayan mountains, Bajracharya et al.¹⁹ estimated a 4% reduction in turbine efficiency of Chilime HPP (2 × 11 MW) for 2 years of continuous operation. In a similar study in Indian Himalayas, Din and Harmain⁹ monitored the sediment characteristics and erosion in a Pelton injector during one monsoon season from May 2017 to September 2017 in the Chenani HPP (5 × 4.66 MW). They observed ploughing action and crater formation due to erosion in the nozzle exit region and in the needle tip region caused by the high impact velocity of the particles. On the other hand, erosion in the form of ripples was observed in the other regions with a lower impact velocity. At Toss HPP (2 × 5 MW) located in the Himalayas, Rai et al.²³ reported an efficiency loss of 7.43% in the Pelton turbine at 80% load due to erosion. These observations help in calibrating the erosion models and validating the numerical simulations; however, estimating the effect of a specific input on the erosion cannot be ascertained from field studies as the inflow conditions of sediment cannot be entirely controlled in HPPs. Further,

each HPP is different with respect to sediment inflow conditions, design head, and discharge.

The hydro-abrasive erosion can be mitigated by constructing a desilting arrangement before the inlet of the penstock; however, due to space and economic constraints in hilly regions, their size is limited and it does not remove 100% particles.²⁴ As a result, during high flow conditions, even large sediment particles with the size of more than 200 μm pass through it and cause erosion.¹⁹ Therefore, other methods such as optimization of design and flow condition as well as the use of high erosion-resistant coating over the turbine material are required to diminish the erosion effect. Tarodiya et al.²⁵ compared the erosion rate of the Pelton injector for a different combination of the nozzle-needle angle in pairs and observed the 110°/70° nozzle-needle pair to be the most optimum. Further, they observed coated Pelton injector with WC-Co-Cr coating on martensitic stainless steel resists 100 times more than an uncoated one. Rai et al.¹⁸ noticed Pelton buckets made of brass to be very sensitive to hydro-abrasive erosion; whereas, 13Cr-4Ni martensitic stainless steel with WC-Co-Cr HVOF coating has the highest resistance to hydro-abrasive erosion. But, before implementing mitigation techniques, quantitative evaluation acquiring data of sediment properties like suspended sediment concentration and particle size distribution are required. The recently developed in situ technologies based on laser diffraction, optical backscattering, and acoustic backscattering can be used for continuous measurement of sediment properties.^{12,26}

Using numerical simulations, the effects of changes in design conditions of turbine components, head, inflow sediments, and material conditions on hydro-abrasive erosion have been studied recently.^{27–30} Further, complex phenomena such as vortex shedding, secondary flow, and cavitation in turbines have also been captured using numerical methods.^{31–33} However, such simulations are rare in the case of Pelton turbines due to complex flow requirements involving the water-air interface, the presence of solid particles, etc. The Pelton injector erodes extensively in plant conditions and is one of the most important components of the Pelton turbine influencing its efficiency. To study the erosion characteristics of an injector with an internal servomotor, Guo et al.²⁸ and Messa et al.³⁴ considered different numerical schemes for the analysis of sediment-laden flow. Guo et al.²⁸ used a Discrete Phase Model (DPM) with a 456 m operating head; whereas, Messa et al.³⁴ applied the STAR CCM + tool for an operating head of 410 m. Both observed similar erosion hotspots for injector components, i.e. nozzle and needle. The maximum erosion in the needle was found at a location a little upstream of the needle tip; whereas, the maximum erosion of the nozzle was found at the exit region. Though Messa et al.³⁴ obtained negative pressure near the nozzle exit, the cavitation modelling is missing from their study. In another similar study, Tarodiya et al.³⁵ adopted CFD-DEM modelling for an operating head of 150 m considering non-uniform sediments to observe asymmetrical erosion patterns. None of the numerical studies considered high-head injector operation above 800 m. In Table 1, the head considered by different researchers while investigating hydro-abrasive erosion in a Pelton injector is provided.

However, these studies on the Pelton injector did not consider the effect of sediment parameters and the head of HPP on the hydro-abrasive erosion rate. Moreover, a study of an injector with an external servomotor considering the DPM model to track particles is rarely available in the literature.

To analyse the erosion characteristics, a study of complex flow conditions in the Pelton injector is essential. Guo et al.²⁸ observed secondary flow due to vortex shedding near the needle guide and a velocity deficit near the needle tip in an injector with an internal servomotor. Han et al.³⁸ found secondary flow creating dean vortices in the distributor part of the Pelton injector while Zhang and Casey³⁹ found secondary flow caused a jet core shift due to a 90° bend pipe in the injector. Often, profile degradation due to erosion leads to local cavitation in Pelton turbine components, predominantly in high-head conditions.^{9,19,40–43} The inception of cavitation increases the material loss rate significantly due to the synergic effect of hydro-abrasive erosion and cavitation resulting in rapid reduction of efficiency.^{42,43} In addition to the eroded profile, part load operating conditions and improper design of the components cause the formation of vortices and secondary flows leading to cavitation. In the Pelton turbine, the needle of the Pelton injector is prone to cavitation during partial load conditions.^{9,19} In addition, cavitation is also observed in the front and cut-out regions of Pelton buckets.^{40,41,43} In the literature, no one has numerically studied the synergic effects of erosion and cavitation though it is observed in the actual injectors of various high-head HPPs.

In this paper, hydro-abrasive erosion of a Pelton injector for a high-head HPP is studied numerically considering a Eulerian-Lagrangian approach. The hydro-abrasive erosion in the Pelton injector with an external servomotor is investigated by varying the head available at the inlet, nozzle opening, and sediment characteristics such as size, concentration, and size distribution. The variation in the operating head, as well as the operating load conditions, are considered to incorporate a wide range of flow conditions. Further, the cavitation model is also implemented to explore the possibility of the synergic effect of cavitation and hydro-abrasive erosion in the injector components. The numerical results conform to the field observations available in the literature. The paper is organised into five sections where first section provides an introduction and details of available literature on the erosion of Pelton turbine components. The sections thereafter describe the details of the study HPP and the numerical scheme used for simulation along with its validation. Finally, the obtained results are discussed in comparing the findings with the literature and last section concludes the study.

Hydro-abrasive erosion in Kashang HPP

The Kashang HPP is a run-of-river HPP located in the Kannur district of Himachal Pradesh, India in the Himalayas operated by 'Himachal Pradesh Power Corporation Limited' (HPPCL). The water from two streams, i.e.

Table 1. Head considered in various literature.

Literature	Head considered (m)
Liu et al. ³⁶	671
Guo et al. ²⁸	456
Messa et al. ³⁴	410
Tarodiya et al. ³⁵	150
Bajracharya et al. ³⁷	30.5

Kashang and Kerang streams - tributaries of the highly sediment-laden Sutlej River is utilised for generating renewable-based electricity. The Kashang HPP has a total installed capacity of 195 MW (3×65 MW) consisting of 3 units of five jet vertical Pelton turbines with 8.99 m³/s unit discharge and a rated head of 820 m. At such a high head, the flow velocity is very high causing local pressure drop and flow separation leading to the possibility of cavitation.^{42,43} As a result, even a small sediment particle causes severe wear and material loss of Pelton turbine components due to the synergic effect of cavitation and hydro-abrasive erosion as shown in Figures 1 and 2. In Figure 2, the severe erosion of one of the injectors operated during a single monsoon season from a new condition is provided. The erosion process alters the profile of turbine components, disturbing the flow pattern, and resulting in reduced generation efficiency of the HPP. As the synergic effect is more prominent in the high head HPPs,^{9,40} the present numerical study attempts to investigate such a complex synergic erosion process corresponding to the head of Kashang HPP, i.e. 820 m. Details of Kashang HPP are mentioned in Table 2.

Methodology

This section presents the governing equations and numerical schemes of ANSYS Fluent applied to model the flow behaviour and hydro-abrasive erosion in the Pelton turbine injector used in the present work.

Geometrical modelling and meshing

As seen in Figure 3, the designs of an injector with an external and internal servomotor are considerably different and therefore have different erosion patterns.²⁸ The design of the Pelton injector with external servomotor considered in the present work consists of a nozzle and needle with 90° and 50° angles, respectively, having a 100 mm nozzle opening diameter (D_0) (Figure 4). In the paper, the nozzle opening is portrayed as a stroke ratio which is a ratio of spear travel (S) to nozzle diameter at exit (D_0). While investigating the effect of sediment parameters and HPP head on hydro-abrasive erosion, the stroke ratio is kept constant at 0.46. The computational domain as shown in Figure 5 includes a pressure inlet, pressure outlet, and wall with smooth no-slip boundary conditions. The pressure inlet is specified according to the required head, zero-gauge pressure is set at the outlet, and operating pressure is taken equal to one atmosphere.



Figure 1. Eroded components of Pelton turbine of high head Kashang HPP (a, b) Needle, (c) Nozzle, (d) Bucket.

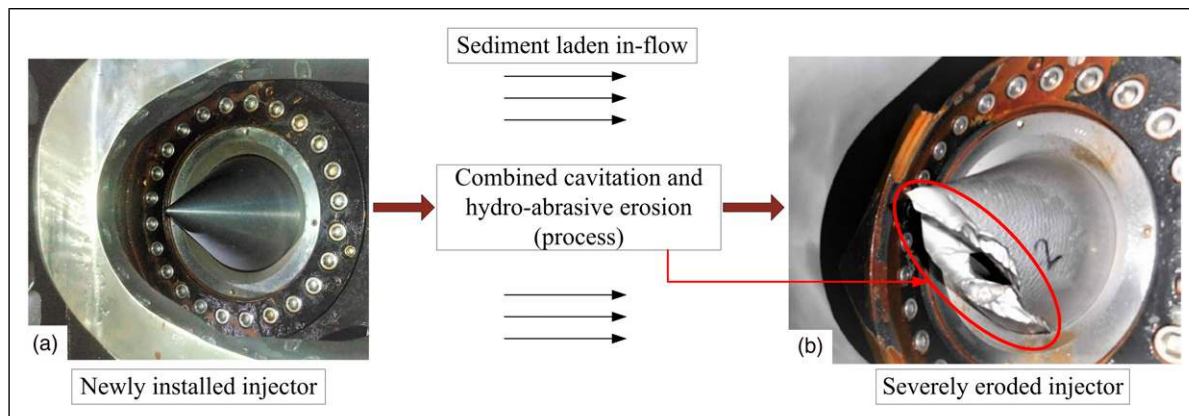


Figure 2. Components of Pelton injector from Kashang HPP (a) before and (b) after the erosion process.

A structured hexahedral mesh of the computation domain was created using the ICEM CFD tool. The minimum value of the quality, determinant $3 \times 3 \times 3$ of the mesh is 0.486. As shown in Figure 6, a fine mesh was created near the surface of the nozzle and needle in order to capture the effect of boundary layer formation. However, the first layer thickness is kept greater than the biggest size sediment particle considered during the simulation for the Discrete Phase Model (DPM) approach to be effective.^{25,35,37,44}

Further, a grid independency test was performed using the 'area average velocity' at the inlet as a reference parameter to check the influence of mesh elements on the numerical results. 2.58 million mesh elements were used for numerical simulation since the reference parameter barely varied with a further increase in mesh elements as shown in Figure 7. Due to the formation of an S-shaped curve in

Table 2. Details of kashang HPP

Specification	Description
Number of units	3 (65 MW each)
Number of injectors	5
Turbine discharge per unit	8.99 m ³ /s
Operating head	820 m
Turbine speed	600 r/min
Nozzle and needle angle	90° and 50°
Material	Turbine steel

Figure 7, the value of area average velocity obtained between 0.5 million and 2 million elements varied significantly. Thus, considering the higher quality of mesh resulting in better accuracy obtained with higher number of mesh elements, a numerical scheme with 2.58 million mesh elements was considered for the simulation.

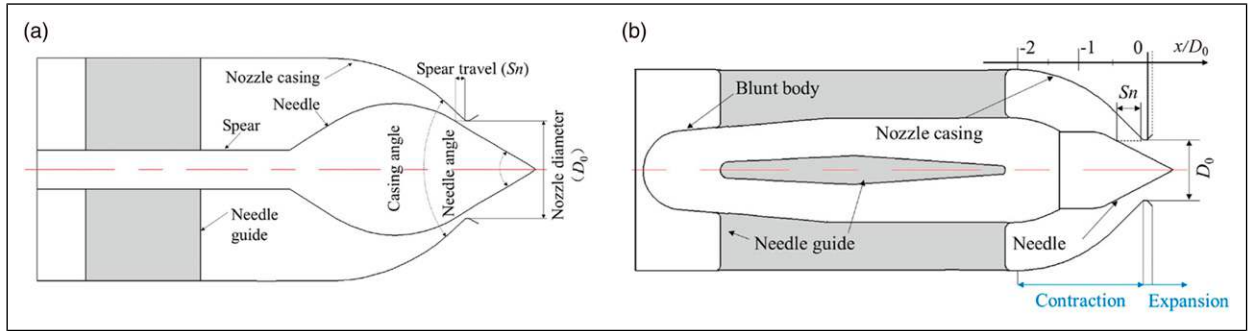


Figure 3. Type of Pelton injector based on its design (a) injector with external servomotor (b) injector with internal servomotor.²⁸

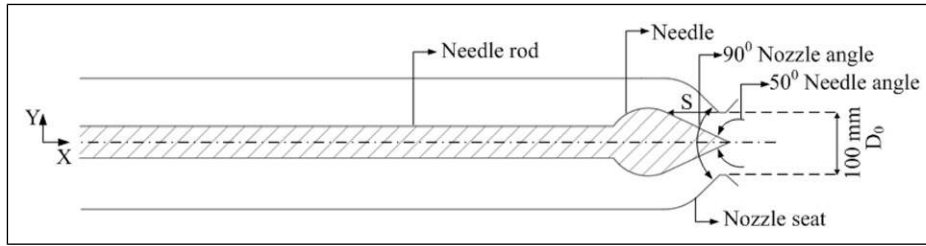


Figure 4. Schematic sketch of Pelton turbine injector.

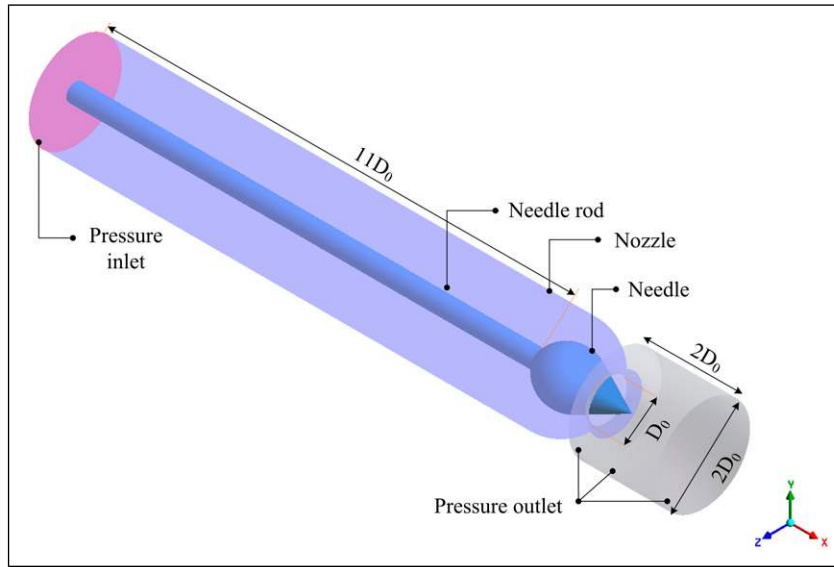


Figure 5. Computation domain of Pelton injector considered for the study.

Governing equations and numerical setup

A total of four different phases were considered in this study. To simulate these four phases which are water-liquid, water-vapour, air, and discrete phase, i.e. sand particles, the multiphase mixture model based on the Euler approach is implemented. For investigating hydro-abrasive erosion, water-liquid, air, and discrete phases are considered; whereas, water-liquid, air, and water-vapor are considered for investigating the cavitation phenomenon. The mixture model considered the interaction of mass and momentum transfer of the inter-phase. Further, the steady-state flow condition is considered during simulation as the flow conditions at a given opening remain constant if other operating parameters do not vary. The volume fraction of

water at the inlet was set to one. The governing equations for this model include continuity and momentum as shown in equations (1) and (2).

$$\nabla \cdot (\rho \vec{U}) = 0 \quad (1)$$

$$\frac{\partial}{\partial t} (\rho \vec{U}) + \rho (\nabla \cdot \vec{U} \vec{U}) = -\nabla p + \nabla \cdot [\mu (\nabla \vec{U} + \nabla \vec{U}^T)] + \nabla \cdot \left(\sum_{x=1}^n \Phi_x \rho_x \vec{U}_{dr,x} \vec{U}_{dr,x} \right) + \vec{F}_B \quad (2)$$

where \vec{U} , ρ , t , p , μ , Φ_x , ρ_x and $\vec{U}_{dr,x}$ represent velocity vector, mass density, pressure, dynamic viscosity, volume

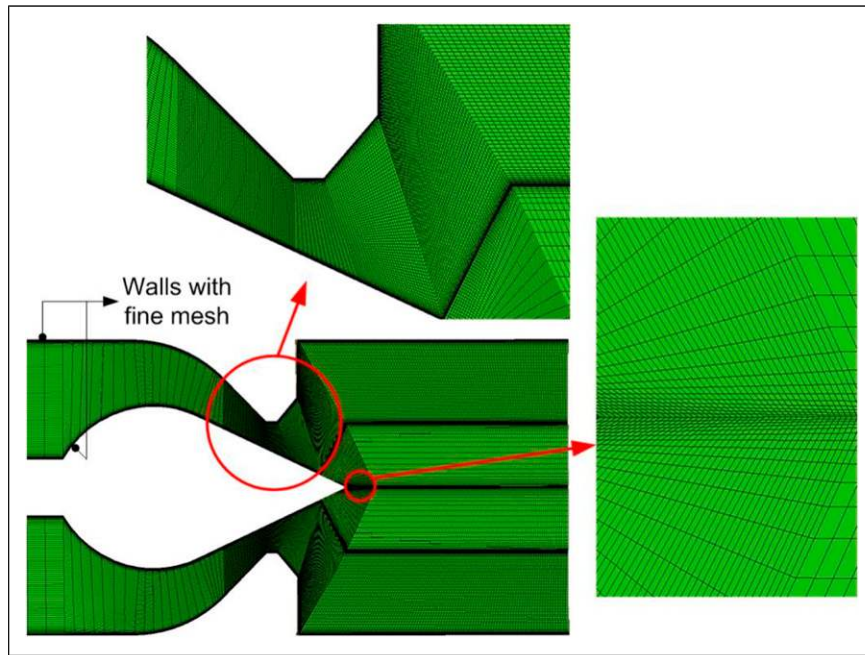


Figure 6. Structured mesh at mid-section plane of Pelton injector.

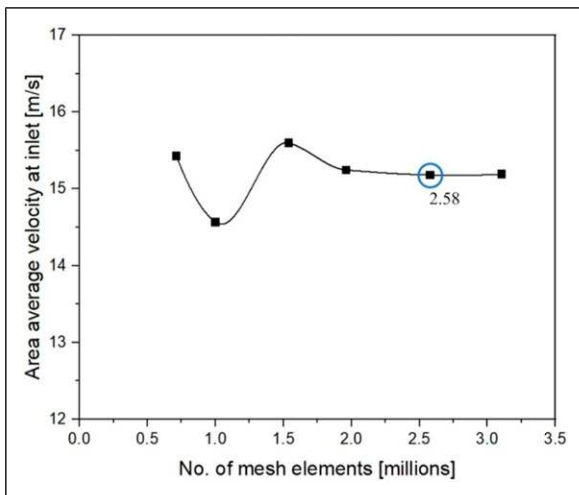


Figure 7. Mesh independence test.

fraction, density, and drift velocity of 'x' secondary phase, respectively; whereas, \vec{F}_B represents body force. For capturing the hydro-abrasive erosion in the injector, an erosion/accretion physical model was applied. For including the turbulence dispersion effect on the dispersed phase, a discrete random walk mode was used. A Lagrangian-based DPM model depicted in equation (3) is used to track sediment particles.²⁸ Reflect type boundary condition was chosen in the DPM model for the wall.

$$\frac{d\vec{V}_p}{dt} = \vec{F}_D(\vec{V} - \vec{V}_p) + \frac{\vec{g}(\rho_p - \rho)}{\rho_p} + \vec{F} \quad (3)$$

where, \vec{V}_p and t represents particle velocity and time, respectively; whereas $\vec{F}_D(\vec{V} - \vec{V}_p)$ term represents the drag

force experienced by a particle having unit mass shown in equation (4) and \vec{F} is additional force per unit particle mass causing fluid acceleration, one of its inclusive force \vec{F}_v i.e. virtual mass force required to accelerate the fluid near the particle is given by equation (5), and the other inclusive force \vec{F}_p arising due to pressure gradient is given by equation (6). It was assumed that the sediment particles had the density of quartz (2650 kg/m^3), which is present in a very high quantity in the water coming to hydropower plants and is a leading cause of hydro-abrasive erosion.^{9,18,19} Since the value of water density to sediment particle density is greater than 0.1, additional forces constituting virtual mass and pressure gradient forces are also considered and are given by equation (6) and equation (7), respectively.⁴⁵

$$F_D = \frac{18\mu C_D \text{Re}}{\rho_p d_p^2 24} \quad (4)$$

$$\vec{F}_v = \frac{1\rho d}{2\rho_p dt} (\vec{V} - \vec{V}_p) \quad (5)$$

$$\vec{F}_p = \frac{\rho}{\rho_p} \vec{V}_p \nabla \vec{V} \quad (6)$$

where, \vec{V}_p , F_D , \vec{V} , \vec{g} , ρ_p , ρ , C_D , Re , and d_p are particle velocity, momentum exchange coefficient, fluid velocity, acceleration due to gravity, particle density, fluid density, drag force coefficient, Reynolds number, and particle diameter, respectively.

In the present study, the Oka erosion model is selected for erosion estimation.⁴⁶⁻⁴⁹ Because, in addition to flow velocity and particle impact angle, Oka erosion model considers the hardness of wall material and particle size, which are not included in the Finnie and McLaury erosion

model available in Fluent making it more accurate.⁴⁵ The erosion rate (E) in the Oka model is determined by equation (7).

$$E = E_{90} \left(\frac{V_1}{V_R} \right)^{k_1} \left(\frac{d_p}{d_R} \right)^{k_2} f(\alpha) \quad (7)$$

where E_{90} is the reference erosion ratio for an impact angle of 90° , V_1 is the impact velocity of a particle, V_R is reference velocity, d_R is reference particle diameter, k_1 is velocity exponent, k_2 is diameter exponent and $f(\alpha)$ is impact angle function obtained using equation (8).

$$f(\alpha) = (\sin \alpha)^{n_1} (1 + H_v(1 - \sin \alpha))^{n_2} \quad (8)$$

where, α , H_v , n_1 , and n_2 are impact angle, Vickers hardness (Gpa) of wall material, and angle function constants, respectively. Particle-wall collision is considered perfectly elastic by taking the coefficient of restitution in a normal and tangential direction equal to unity, after discovering the minor influence of these parameters upon the quantities of interest for this study.³⁴ Generally, for sediment concentration values less than 1% (10,000 ppm), one-way coupling

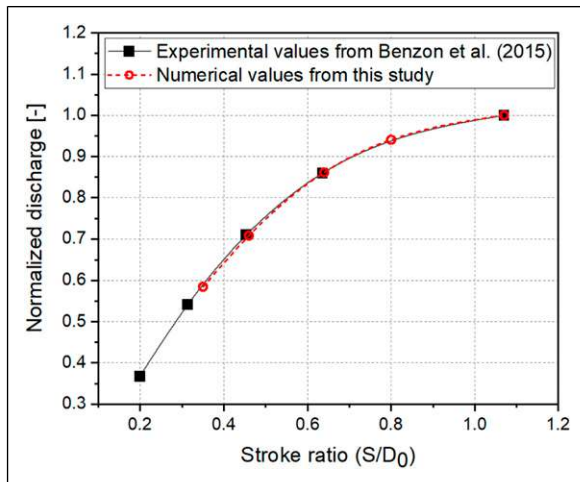


Figure 8. Variation of normalized discharge with respect to stroke ratio.

can be used for reasonable accurate results while investigating hydro-abrasive erosion in a Pelton injector.³⁴ However, in the present study, a two-way coupling approach is considered by enabling the ‘interaction with continuous phase’ option in the DPM panel to capture the interaction between various phases more effectively and to observe the effect of the discrete phase on the continuous phase and vice versa. For solving kinetic energy and turbulent frequency, the SST $K-\omega$ turbulence model was implemented since the SST $k-\omega$ model provides benefits of both standard $k-\epsilon$ and $k-\omega$ by switching between $k-\epsilon$ away from the wall and $k-\omega$ near the wall using the blending function. Pressure-velocity linking was accomplished through a coupled scheme. While investigating the effect of sediment size distribution on hydro-abrasive erosion rate, the distribution of mass of different sediment sizes is considered according to the Rosin-Rammler function.⁵⁰ For capturing the water-vapour, the Schnerr-Sauer cavitation model is considered; water-vapour volume fraction (Φ_v) according to Schnerr and Sauer⁵¹ is given by equation (9).

$$\Phi_v = \frac{V_v}{V_E} = \frac{\frac{4}{3}\pi R^3 \cdot n}{1 + \frac{4}{3}\pi R^3 \cdot n} \quad (9)$$

where, V_v , V_E , R and n represent the volume of water-vapour in a mesh element, volume of mesh element, radius of water-vapour bubble, and bubble number density, respectively.

Validation of the numerical scheme

To confirm the accuracy of the numerical scheme, the variation of normalized flow rate with the stroke ratio was compared with the experimentally observed values of Benzon et al.⁵² for the 150 m of the head. The results obtained were in good agreement with experimental values⁵² as shown in Figure 8, where normalized discharge refers to the ratio of the local flow rate to the maximum obtained flow rate.

For a fixed nozzle opening of 0.46 stroke ratio, flow velocity increases downstream as fluid moves along the needle tip (Figure 9(a)). Similar results were observed in the

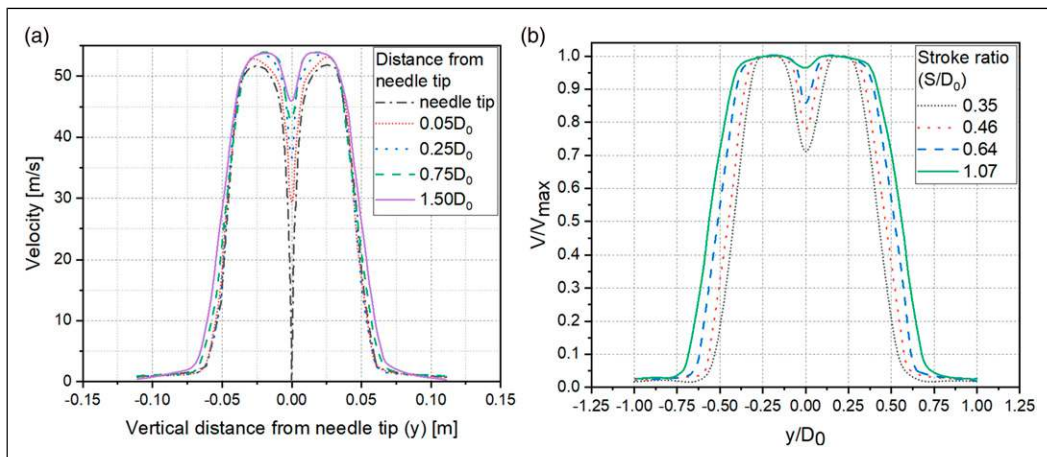


Figure 9. (a) Variation of flow velocity with respect to radial distance, for 0.46 stroke ratio at 150 m of the head, (b) Variation of velocity ratio with respect to the radial position at a distance of ‘ $1D_0$ ’ from the nozzle exit.

experimental study of Zhang and Casey³⁹; and at the needle tip flow velocity is zero similar to Bajracharya et al.³⁷ Furthermore, to examine the effect of nozzle opening on the flow velocity in the injector, the normalized flow velocity based on the ratio of local velocity to maximum possible velocity is plotted with respect to the ratio of radial distance (y) and nozzle diameter (D_0), for a distance of ' D_0 ' mm from the nozzle exit (Figure 9(b)). Increasing nozzle opening increased velocity along the needle tip as the boundary layer effect was reduced, similar results were observed in the study of Jeon et al.⁵³

As sediment-laden water enters the injector, its velocity increases continuously due to a reduction in cross-section.

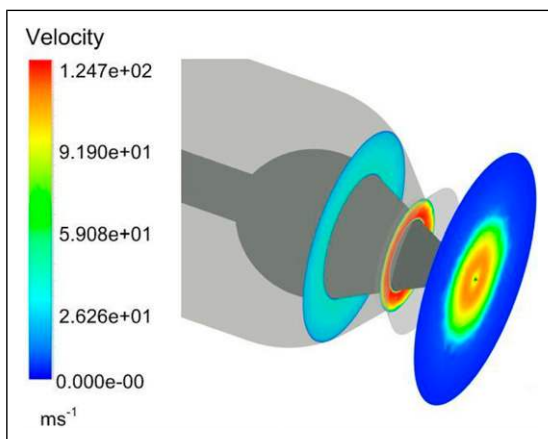


Figure 10. Variation of flow velocity in the Pelton injector along the axial direction.

However, such an increase in velocity continues only up to a location a little upstream of the needle tip. A sudden reduction of velocity takes place at the needle tip due to boundary layer formation reducing the erosion rate simultaneously. For the nozzle, flow velocity continuously increases till the nozzle exit, making it an erosion hotspot as shown in Figure 10.^{28,34} Successful validation of the erosion intensity in different regions of the nozzle and needle was accomplished in the numerical model by taking geometry and sediment properties similar to the field study⁹ as shown in Figure 11. To further analyse it, the erosion rate was plotted lengthwise a strip created along the surface of the nozzle and the needle. The variation of erosion intensity in both nozzle and needle along the axial direction was similar to Guo et al.²⁸ as shown in Figure 12. Therefore, the numerical scheme used in this study is found to accurately capture erosion phenomena. Various parameters considered during this study along with their respective variations are presented in Table 3.

Results and discussion

The effects of various parameters obtained from numerical simulation in this study related to sediment, flow, and operating parameters on erosion rate are presented in this section along with cavitation assessment on the injector. As a significant difference in erosion pattern is observed in injectors with internal and external servomotors, the analysis of the erosion patterns with the flow behaviour is also explored and discussed with the available literature.

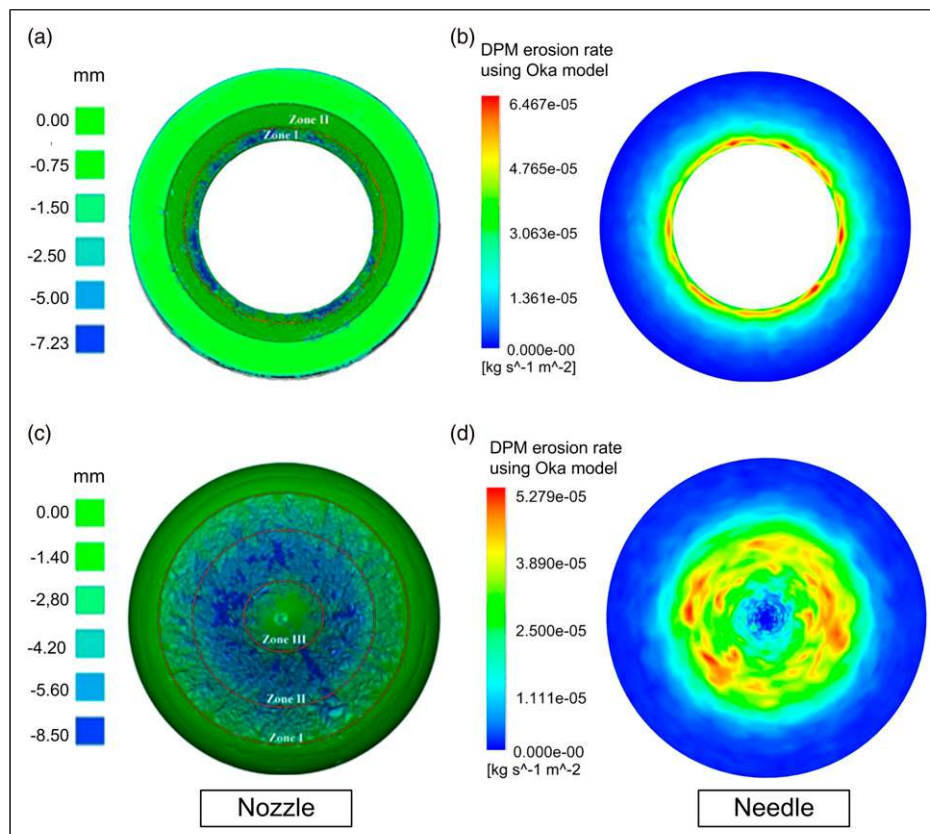


Figure 11. Front view of eroded nozzle and needle (a, c) Field study of Din and Harmain,⁹ (b, d) Numerically obtained.

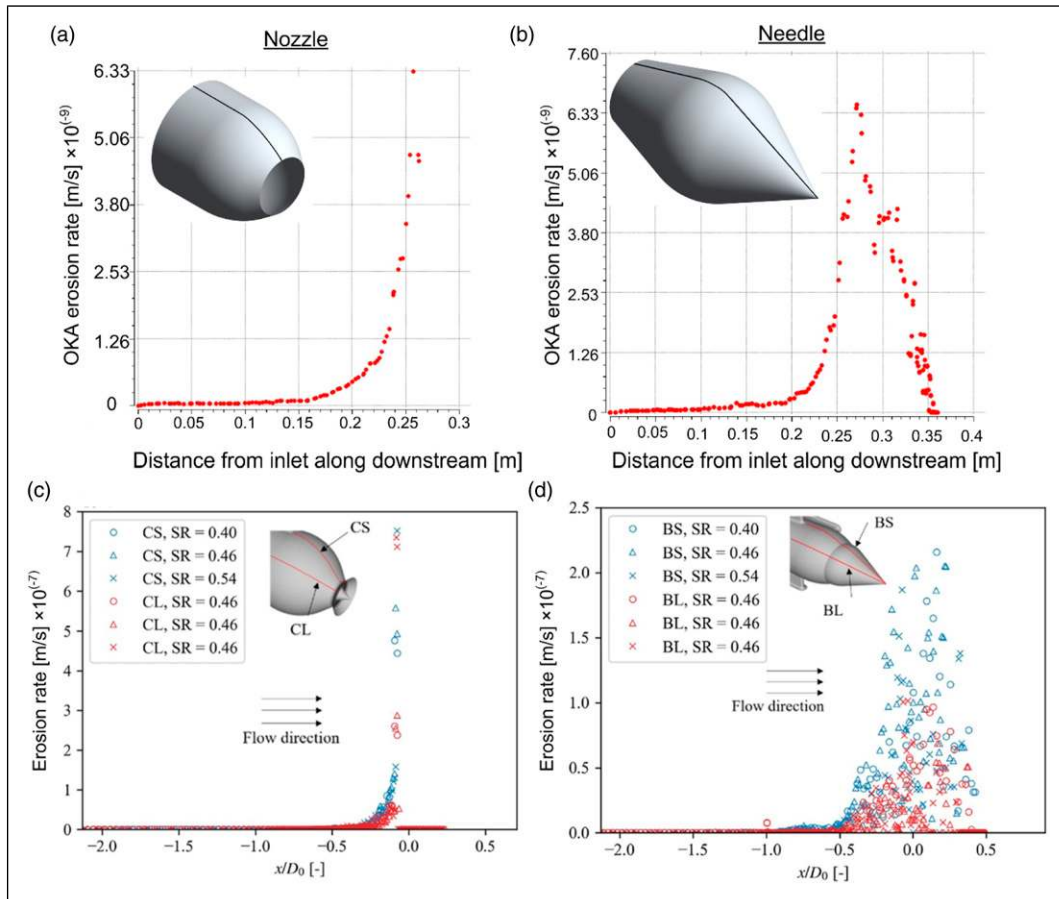


Figure 12. Variation of erosion along the axial direction in (a, c) nozzle and (b, d) needle, observed in this study (a, b) and by Guo et al.²⁸ (c, d).

Table 3. Sediment, flow, and operating parameters considered in the study.

Parametric variation considered	Parameter fixed during a particular simulation			
	Sediment size	Sediment concentration	Head	Stroke ratio
Sediment size 3 values (40 μm, 100 μm, 200 μm)	–	750 ppm	820 m	0.46
Sediment concentration 3 values (750 ppm, 1500 ppm, 3000 ppm)	40 μm	–	820 m	0.46
Head 4 values (200 m, 360 m, 600 m, 820 m)	40 μm	750 ppm	–	0.46
Stroke ratio 4 values (0.35, 0.46, 0.64, 0.8)	40 μm	750 ppm	820 m	–

Effect of sediment size

In sediment-laden water, particles of different sizes are present and a particular size of sediment has a different effect on both the rate as well as the pattern of erosion in a Pelton injector.^{36,41} Generally, the sediment size reaching turbine components passing through the desilting basin is below 200 μm in HPP. However, desilting basins are not 100% efficient especially during the monsoon season due to the high influx of sediment and particles with size more than 200 μm also entering the turbine components. The bigger sediment size particles lead to a higher erosion rate in the nozzle as shown in Figures 13 and 14. This is because the bigger sediment particles strike the nozzle surface with higher kinetic energy. Moreover, for bigger sediment size particles, the formation of erosion ring is observed at just the start of the convergent region. This is because higher inertia of bigger size sediment particles leads to a higher separation angle from curved streamlines.¹⁶ In the case of

the needle, the erosion rate decreases with an increase in sediment size as shown in Figures 13 and 14, also observed in the study of Liu et al.³⁶ This is because smaller sediment particles follow the fluid streamlines more closely due to less inertia and strike the region of the needle corresponding to high flow velocity resulting in a high erosion rate as shown in Figure 15. Whereas, most of the bigger sediment particles resist the change in flow path and strike near the needle neck due to high inertia. Thereafter, the bigger particles are separated from the streamlines and leave the injector without striking the needle corresponding to the high flow region upstream of needle tip as shown in Figure 15. From Figure 15, it is inferred that 40 μm size particles follow the streamlines more closely compared to 200 μm size particles. As the flow velocity is less near the needle neck region due to a higher flow cross-section, even the higher number of impacts from bigger size particles does not cause considerable erosion as shown in Figure 13(e) and (f).

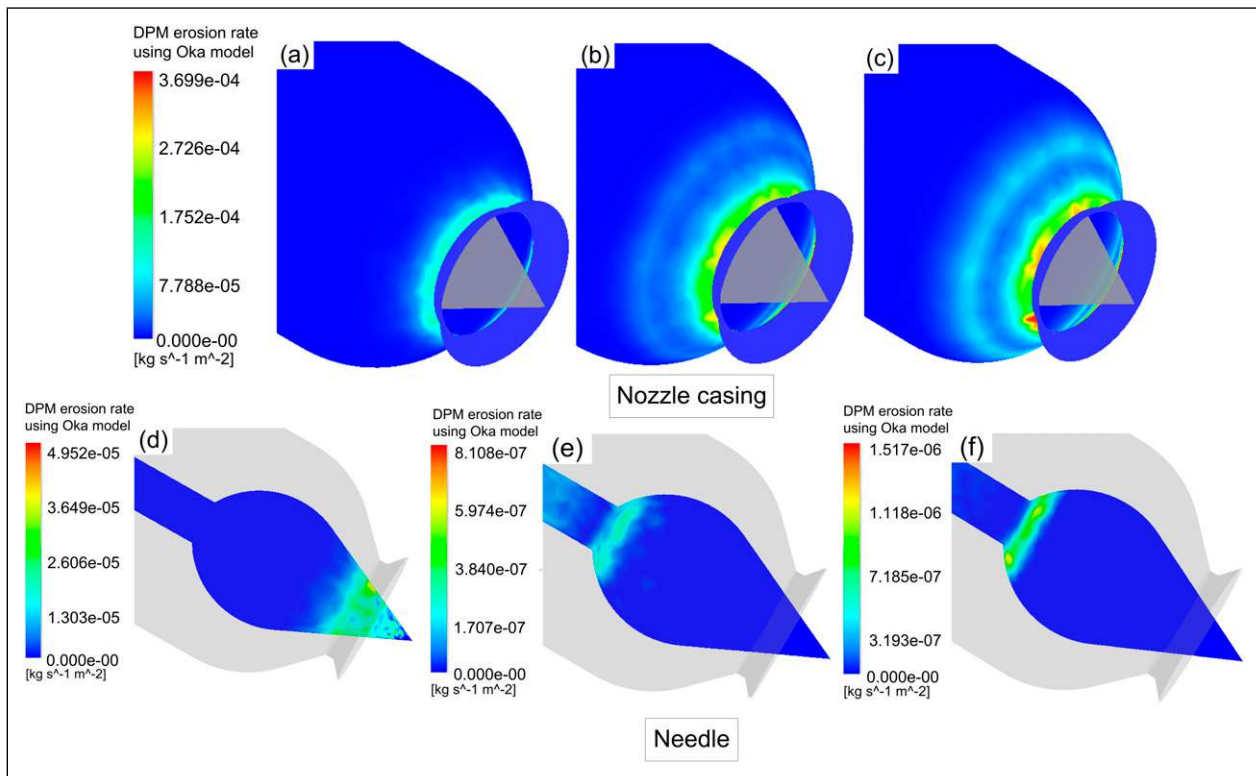


Figure 13. Erosion rate on nozzle casing and needle at sediment size values (a, d) 40 μm, (b, e) 100 μm, and (c, f) 200 μm.

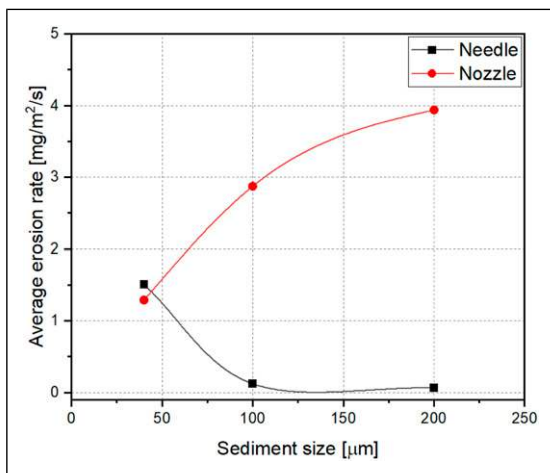


Figure 14. Variation of average erosion rate with respect to sediment size.

Effect of sediment concentration

Sediment concentration is at its highest during rainy or snow-melt seasons, resulting in a higher rate of erosion in turbine components like injectors. Din and Harmain⁹ reported a maximum concentration of 2000 ppm at Chenani HPP in 2017; whereas, Boes⁵⁴ observed it to be 5000 ppm at Dorferbach HPP in 2008. The maximum value of the concentration can go as high as 60,000 ppm.^{6,22} However, HPPs are closed prior to such highly concentrated sediment-laden water coming in contact with critical components of the turbine as a mitigation measure. Therefore, the average and maximum sediment concentrations generally lie around 1000 ppm and 3000 ppm, respectively.^{9,18} Based on Figure 16, it is seen that erosion

rates in both needles and nozzles increase as concentration increases. This enhancement of erosion rate is due to an increase in the number of particles striking the surface per unit area while the size of sediment particles remains constant i.e. 40 μm. In both the nozzle and needle, average erosion rates increase linearly with concentration, as shown in Figure 17. Similar results were observed in the experiments of Padhy and Saini¹⁵ and Rai et al.¹⁶ for various materials including turbine steel. Further, IEC 6234⁵⁵ also suggested adopting a linear relation between erosion and sediment concentration in its empirical relation for erosion depth. This linear trend in variation of erosion is due to 'n' times increase in the possibility of the number of sediment particles striking the unit area on increasing the sediment concentration by 'n' times. To operate a plant at optimum levels in erosive conditions, a cut-off limiting concentration value should be decided for every plant as plant components can be severely damaged at higher concentrations.¹⁶ Among a few such attempts to obtain limiting concentration value for a hydropower plant, Boes⁵⁴ and Felix²² estimated cut-off concentrations to be 1100 ppm and 1000 ppm for Dorferbach HPP and Fieschertal HPP, respectively.

Effect of head of a hydropower plant

The head of an HPP is a design parameter of an HPP affecting the erosion process, as the head is directly proportional to the square root of the flow velocity and the flow velocity is the most dominating parameter affecting the erosion of Pelton turbines.¹⁶ To determine the effect of the plant design head on the erosion of the injector, the head was varied between 200 m and 820 m by changing the pressure condition at the inlet in

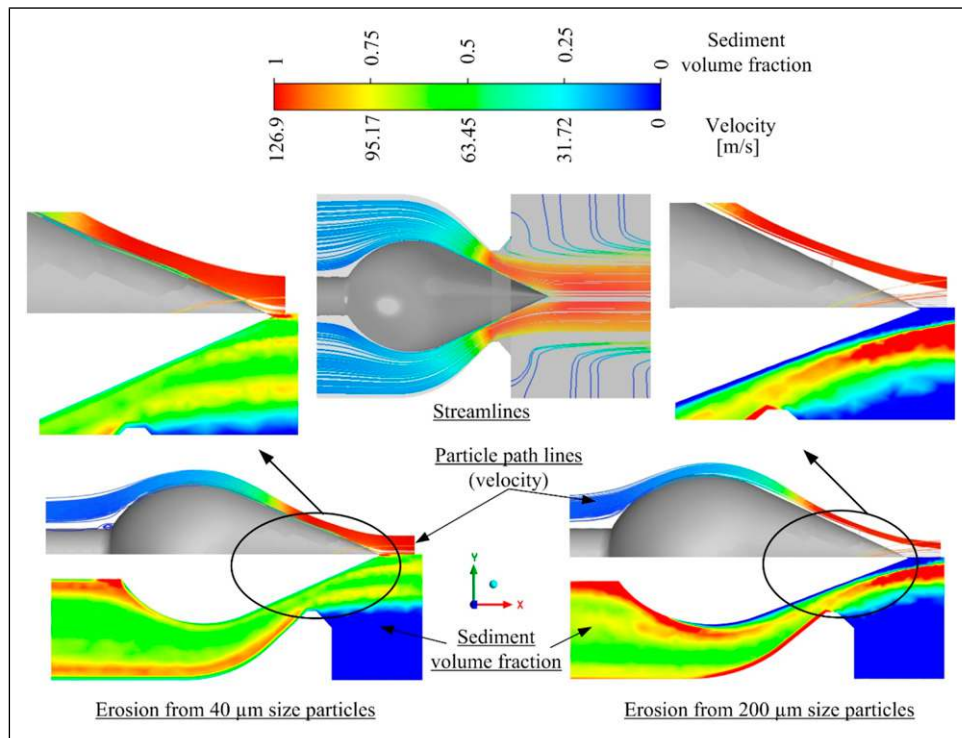


Figure 15. Particle path lines and sediment volume fraction for 40 μm and 200 μm size sediment particles.

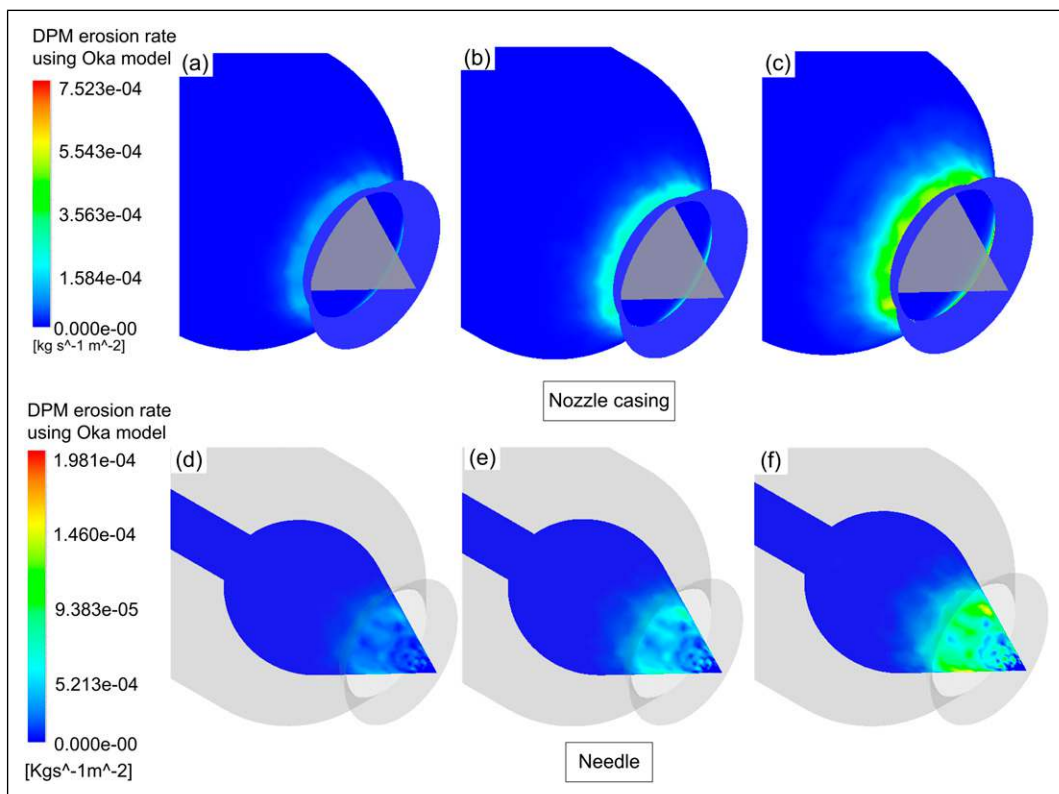


Figure 16. Erosion rate on nozzle casing and needle at sediment concentrations (a, d) 750 ppm, (b, e) 1500 ppm, and (c, f) 3000 ppm.

this study. The Reynolds number (Re) at inlet condition for different heads considered in this study are presented in Table 4. Usually, Pelton turbines are deployed in hydropower plants with high heads varying between 150 m and 1300 m.⁵⁶ As a Pelton injector can be used to cover a wide range of heads, the head variation between 200 m and 820 m is

selected. Further, erosion values from two HPP having 360 m and 820 m heads, i.e. Chenani HPP⁹ and Kashang HPP, are also considered for analysing the findings. Pelton turbine converts pressure energy into kinetic energy before hitting the buckets, which is why a variation in the head can also be viewed as a variation in the flow velocity.

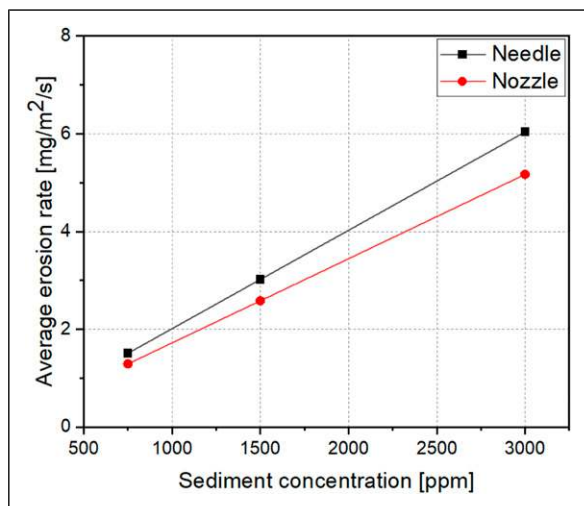


Figure 17. Variation of average erosion rate with respect to sediment concentration.

With the head increase, both the nozzle and needle erosion rate increase as shown in Figure 18(a)–(h). This is due to an increase in the impact velocity of sediment particles striking the injector surface with higher kinetic energy. Rai et al.¹⁶ as well as Padhy and Saini¹⁵ also observed an increase in erosion rate with an increase in flow velocity while performing the experiments on the Pelton turbines. When the head is increased, the average erosion of the nozzle and needle is steeply increased (Figure 19). As a result, HPPs utilizing higher heads like Kashang HPP are more prone to hydro-abrasive erosion as shown in Figure 2. Due to low head and flow velocities, the Kaplan turbine experiences less erosion compared to high-head Pelton and medium-head Francis turbines.⁵ The eroded image of the nozzle and needle from the Chenani HPP is shown in Figure 18(i) and (j) respectively. All the studies, relating the erosion rate of the Pelton turbine with sediment and impact parameters, found the exponent of jet velocity to be maximum with its value between two and 4.⁵⁵

Effect of nozzle opening

The erosion in a Pelton turbine is also affected by operating parameters, like nozzle opening. As the opening of the nozzle is increased, the erosion rate in the nozzle varies minimally as shown in Figure 20(a)–(d), but in the case of a needle, it decreases to a perceptible level, as shown in Figure 20(e)–(h). A similar variation in the erosion rate of the nozzle and needle with nozzle opening was observed by Messa et al.³⁴ On the nozzle, there is a wavy pattern of average erosion rate, whereas, on the needle, a steep drop occurs initially, and then the rate of decrease of average erosion rate decreases as shown in Figure 21. As the nozzle opening increases, the flow area between the nozzle and needle surface increases, reducing the mean flow velocity¹⁹ leading to reduced erosion rate; but, at the same time, the mass flow rate of the particle also increases enhancing the erosion rate. Therefore, the overall change in erosion rate with nozzle

Table 4. Fluid-flow Reynolds number (Re) for different heads considered in the study.

Head considered (m)	Re
200	13.74×10^5
360	18.17×10^5
600	23.33×10^5
820	27.29×10^5

opening depends on the more dominating factor. In the nozzle, the drop in average erosion rate, from stroke ratio 0.35 to 0.46 is due to the dominance of reduction in mean flow velocity, but with further nozzle opening, an increase in mass flow rate becomes the dominant factor enhancing the erosion rate. However, the overall change in the erosion rate of the nozzle with a change in the stroke ratio from 0.35 to 0.8 is quite minimal. In needle, the effect on erosion due to a reduction in mean flow velocity, with an increase in nozzle opening is more dominant causing a steep drop in average erosion rate from stroke ratio 0.35 to 0.8. Similar to the present study, Bajracharya et al.¹⁹ and Din and Harmain⁹ observed the needle to be more susceptible to erosion during partial nozzle opening compared with full nozzle opening. This is mainly due to higher mean flow velocity and inception of cavitation in partial nozzle opening conditions. Severe erosion in the needle of Kashang HPP at part load condition due to the synergic effect of cavitation and hydro-abrasive erosion can be observed as shown in Figure 2. Figure 20(i) shows a severely eroded needle of Chilime HPP due to the synergic effect of cavitation and hydro-abrasive erosion. It is also observed that the region in the needle corresponding to maximum erosion shifts towards the needle tip with an increase in nozzle opening; a similar result was also noted by Tarodiya et al.³⁵ The Reynolds number (Re) at inlet condition for different stroke ratios considered in this study are presented in Table 5.

Effect of sediment size distribution

In the field conditions, the sediment coming with the inflow comprises particles of different sizes and is characterised using particle size distribution (PSD). Thus, to incorporate the effects of the size variation on hydro-abrasive erosion, PSD is considered as shown in Table 6 and Figures 22–25 for 820 m head, 750 ppm sediment concentration, and 0.46 stroke ratio. In general, most of the sediment entering a Pelton turbine has a size of less than 200 μm due to desilting basins in the waterways. However, in high sediment concentration flow conditions, sediment size greater than 200 μm can also enter the turbine components.^{9,18,19,21} Thus, to incorporate the extreme cases, a mean sediment size of 200 μm is also considered in this study in addition to 40 μm and 100 μm . For the mean sediment size of 40 μm , the location of hydro-abrasive erosion remains the same for all the range

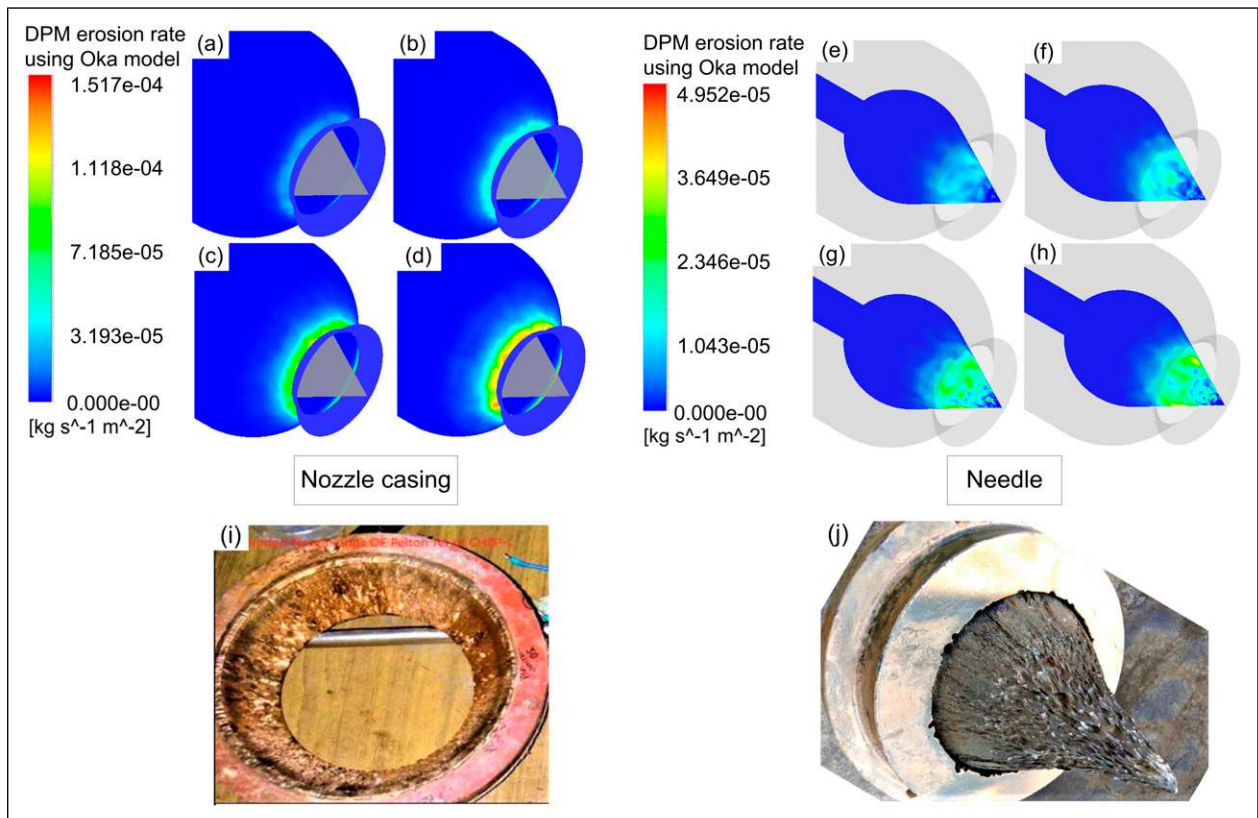


Figure 18. Erosion rate on nozzle casing and needle at head values (a, e) 200 m, (b, f) 360 m, (c, g) 600 m, and (d, h) 820 m, and eroded image of (i) nozzle⁵⁷ and (j) needle⁵⁶ of Chenani HPP.

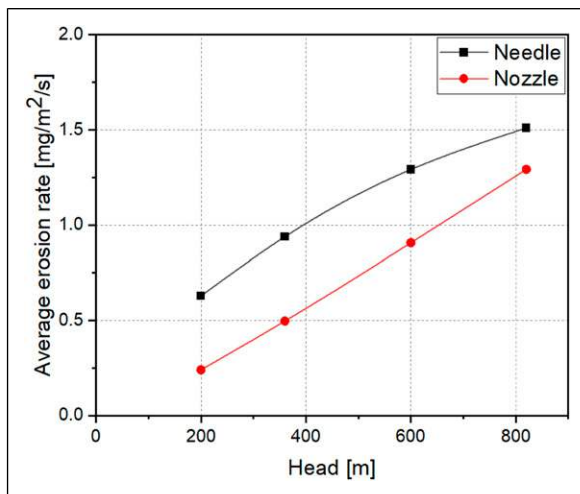


Figure 19. Variation of average erosion rate with respect to the head.

of PSD, i.e. nozzle exit and near little upstream to the needle tip as shown in Figure 22. Messa et al.³⁴ also observed erosion on the same location by taking sediment size of 50 μm . Further, with an increase in the range of sediment size, hydro-abrasive erosion in both nozzle and needle increases as shown in Figure 22.

In the case of PSD with a mean size 100 μm , hydro-abrasive erosion rings are formed near the convergent

region of the nozzle for all the cases of size variation as shown in Figure 23 mainly due to the separation of sediment particles from streamlines. It is observed that hydro-abrasive erosion in the nozzle is less when PSD is considered compared to 100 μm mono-sized particles as shown in Figure 25. Further, hydro-abrasive erosion is only observed in the neck region of the needle for 100 μm mono-sized particles. When broad PSD is considered, the erosion pattern is observed at regions little upstream to the needle tip, which further increases with an increase in the range of sediment size distribution as shown in Figures 23 and 25. This is mainly due to the involvement of smaller sediment size in the erosion process indicating that the smaller size sediments have a higher tendency to hit little upstream to the needle tip; whereas, the larger size sediments have a higher tendency to hit at the needle neck, similar to Tarodiya et al.²⁵ The variation in hydro-abrasive erosion with PSD for a mean sediment size of 200 μm is shown in Figures 24 and 25, which is similar to the erosion with 100 μm . However, due to bigger particles in PSD with a mean particle size of 200 μm , the maximum erosion occurs in the neck side of the needle; whereas, in PSD with a mean particle size of 100 μm , erosion is mostly near the upstream of needle tip as shown in Figures 23 and 24 due to presence of a greater number of smaller particle size. Moreover, hydro-abrasive erosion is more severe in the nozzle and less severe in the needle for 200 μm as compared to respective cases of 100 μm mean PSD as

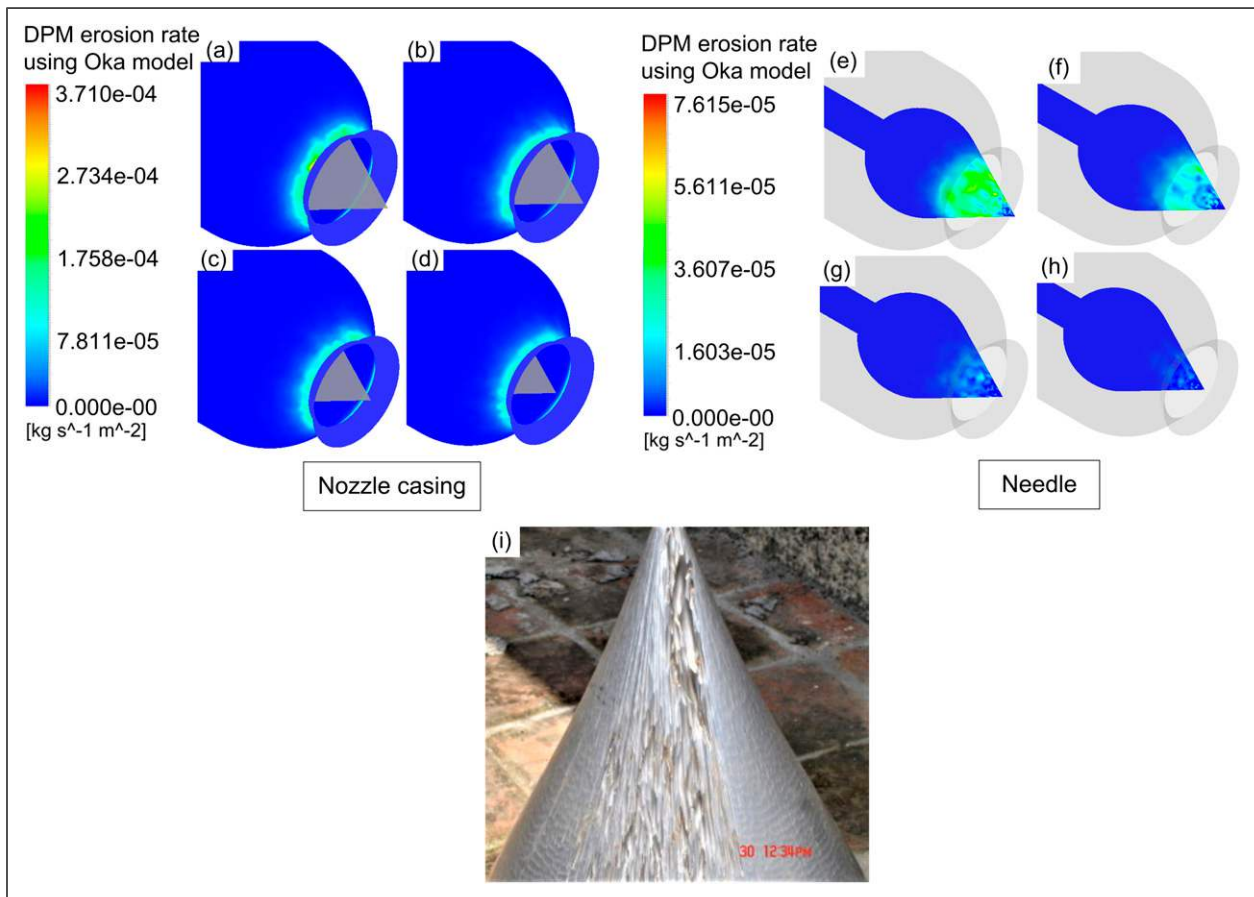


Figure 20. Erosion rate on nozzle casing and needle at stroke ratio (a, e) 0.35, (b, f) 0.46, (c, g) 0.64, and (d, h) 0.8, and (i) severely eroded needle of Chilme H.P.P. at partial opening condition.¹⁹

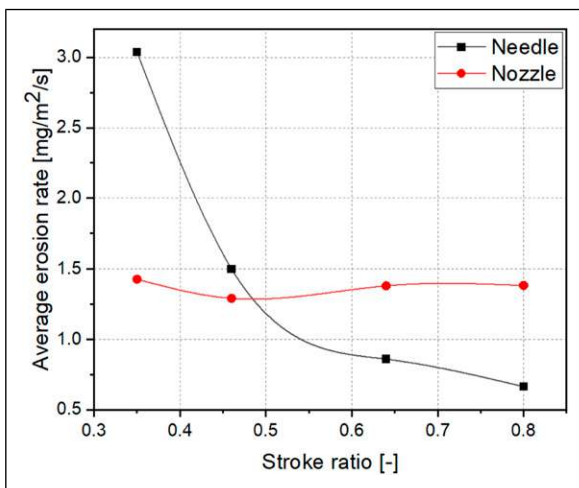


Figure 21. Variation of average erosion rate with respect to stroke ratio.

Table 5. Fluid-flow Reynolds number (Re) for different stroke ratios considered in the study.

Stroke ratio	Re
0.35	23.38×10^5
0.46	27.29×10^5
0.64	33.69×10^5
0.8	36.85×10^5

shown in Figure 24. Such observation in the variation of erosion due to different PSD values is an interesting finding which assists a designer to focus on specific regions of the Pelton components based on the type of size variations expected at the actual plant.

Susceptibility to cavitation

From the numerical investigation, a region of low pressure below vapour pressure of water is observed to form near the nozzle ring due to a sudden contraction of the nozzle. Thus, the cavitation model is implemented for further analysis and water-vapour formation is captured as shown in Figure 26. In general, at higher flow velocities, the possibility of cavitation increases due to a reduction in pressure.^{58,59} As the flow velocity is related to the head of HPP, the effect of the HPP head on the possibility of occurrence of cavitation is investigated for head values from 200 m to 1200 m. Through the cavitation modelling, the volume fraction of water-vapour was found to increase with an increase in head indicating a greater number of bubble formations as shown in Figure 26. Further, as shown in Figure 26, two different slopes are observed for the water-vapour volume fraction curve. As the head increases from 200 m to 600 m slight increase of 6.8% in water-vapour volume fraction is observed; however, as the head further increases from 600 m to 1200 m, the water-vapour fraction increases rapidly by 42%. Hence, the injectors of Pelton turbine in HPPs

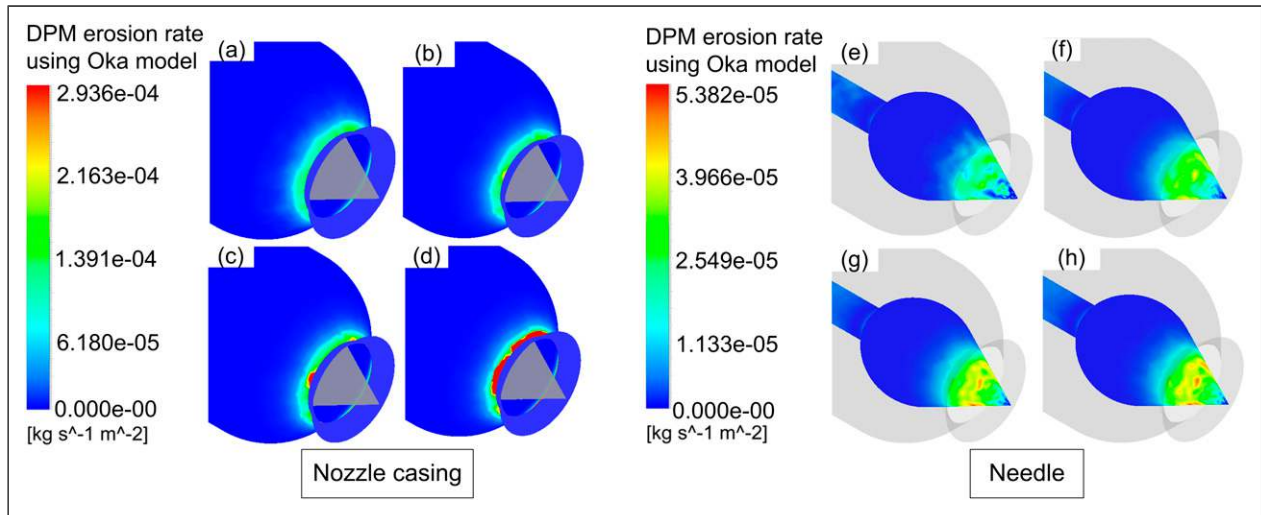


Figure 22. Erosion rate on nozzle casing and needle with 40 μm mean size for different range of sediment size distribution (a, e) mono-sized, (b, f) Medium, (c, g) Broad, (d, h) Very broad.

Table 6. Variation considered in sediment size distribution.

PSD range considered	Particle diameter in μm		
	Min.	Mean	Max.
Mono-sized PSD	40	40	40
Medium-sized PSD	24	40	56
Broad-sized PSD	8	40	72
Very broad-sized PSD	2	40	78
Mono-sized PSD	100	100	100
Medium-sized PSD	60	100	140
Broad-sized PSD	20	100	180
Very broad-sized PSD	5	100	195
Mono-sized PSD	200	200	200
Medium-sized PSD	120	200	280
Broad-sized PSD	40	200	360
Very broad-sized PSD	10	200	390

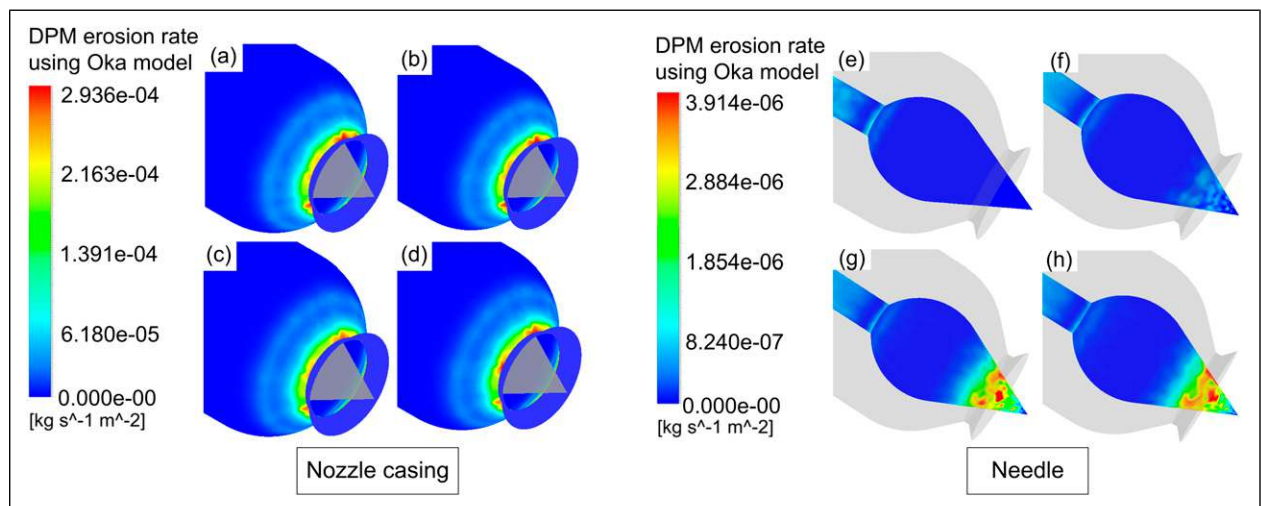


Figure 23. Erosion rate on nozzle casing and needle with 100 μm mean size for different range of sediment size distribution (a, e) mono-sized, (b, f) Medium, (c, g) Broad, (d, h) Very broad.

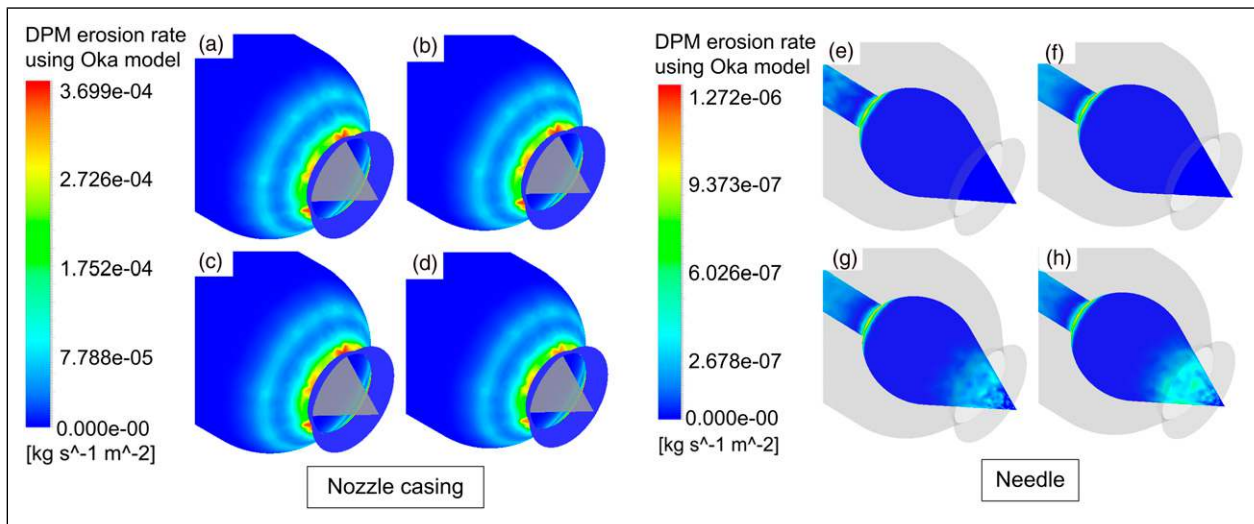


Figure 24. Erosion rate on nozzle casing with 200 μm mean size for different range of sediment size distribution (a, e) mono-sized, (b, f) Medium, (c, g) Broad, (d, h) Very broad.

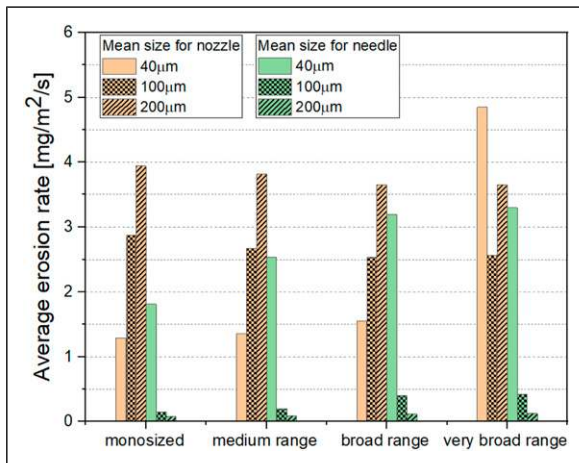


Figure 25. Variation of average erosion rate with sediment size distribution.

designed for higher head values are more prone to cavitation, especially above 600 m.

Synergy of hydro-abrasive erosion and cavitation

Cavitation and hydro-abrasive erosion act as a catalyst to each other increasing the material loss from the components. The hydro-abrasive erosion results in a change of profile of the Pelton turbine, which may cause favourable conditions for cavitation to occur. On the other hand, the collapsing of bubbles increases the impact velocity of sediment particles which further enhances the hydro-abrasive erosion rate.^{42,43} As shown in Figure 27, the region of water-vapour formation coincides with the region with the maximum hydro-abrasive erosion in the nozzle by Din and Harmain,⁹ i.e. Zone I as shown in Figure 11(a) and Figure 27(c). The maximum damage at the nozzle exit is mainly due to the synergic effect of cavitation and hydro-

abrasive erosion which prevails at part load conditions, also observed by Din and Harmain⁹. Further, as shown in Figure 26, along with the water-vapour volume fraction, the hydro-abrasive erosion rate also increases steeply with increase in the head of HPP for the nozzle. Hence, the possibility of wear due to the synergic effect of hydro-abrasive erosion and cavitation in the nozzle increases with the head causing severe damage to the injector of the higher head HPPs. However, in needle due to lesser rate in increase of erosion rate compared to nozzle, the possibility for synergic effect of hydro-abrasive erosion and cavitation is lower as shown in Figure 26. From numerical modelling, the maximum water-vapour volume fraction obtained for 1200 m head was 66%, which is not a sufficient condition for pitting erosion through cavitation as mentioned by Rossetti et al.⁴⁰ The present numerical analysis attempts to locate the most potent region, which has a high possibility for the occurrence of cavitation pitting in the nozzle with a change in operating conditions as well as the distortion of profile because of hydro-abrasive erosion. The same location is found to have the maximum possibility of severe wear due to the synergic effect of cavitation and hydro-abrasive erosion.

Other than sediment and operating parameters, the design of an injector also plays a major role in its performance in hydro-abrasive erosion conditions.^{25,34,60} By reducing the needle angle, more pronounced erosion of the injector was observed.^{34,60} In such conditions, the needle was affected more than the nozzle.⁶⁰ In addition to the nozzle-needle angles, the flow changes due to upstream components from the injector like bend in the penstock pipe significantly affects the pattern and intensity of the erosion in a Pelton injector.⁶⁰ Therefore, design parameters should also be considered and investigated in optimizing the injector for different conditions with potential hydro-abrasive erosion at a site before manufacturing the prototype turbine. This can be achieved by modelling the injector with various

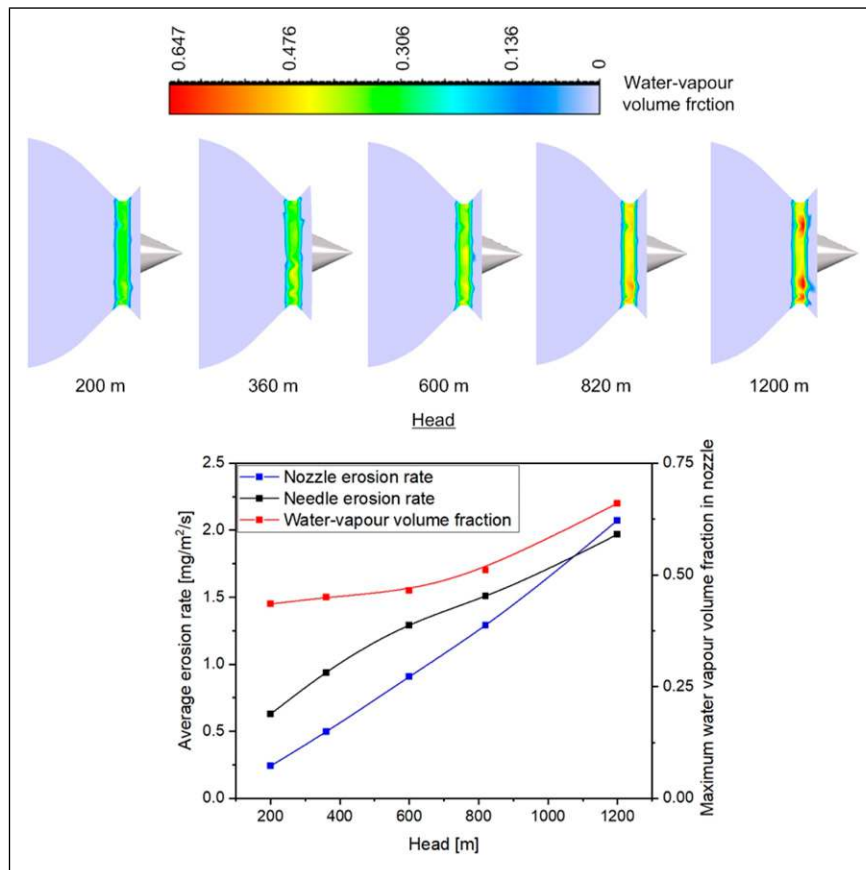


Figure 26. Variation in water-vapour volume fraction in nozzle with head.

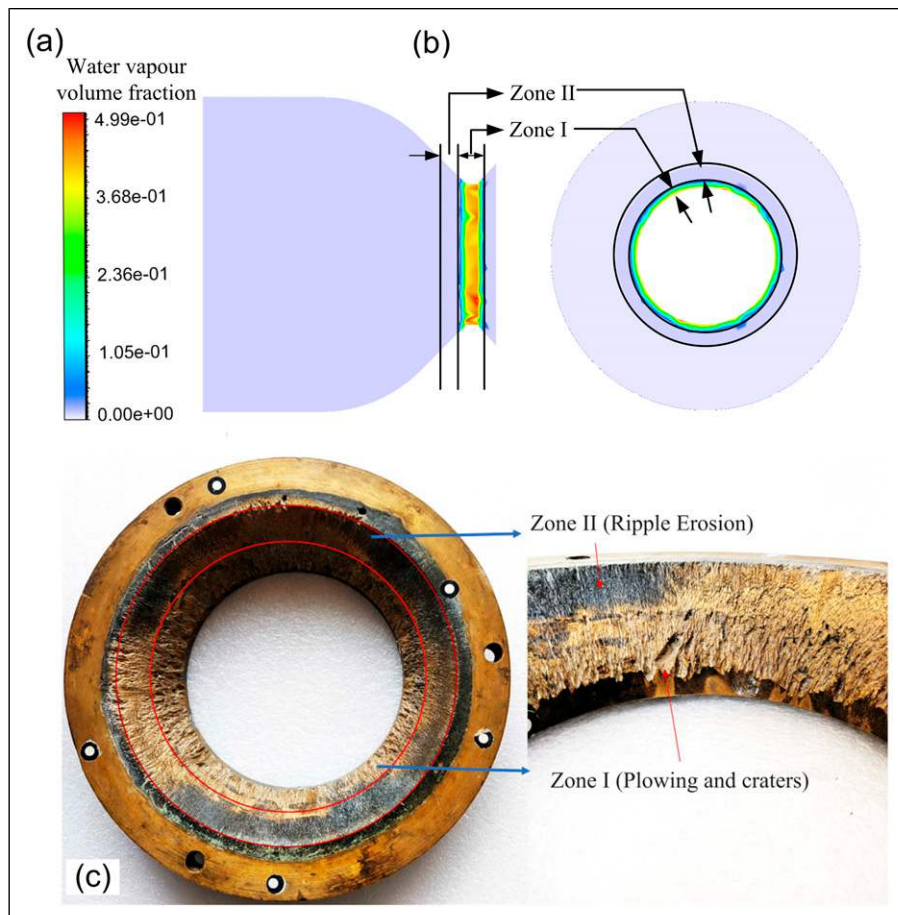


Figure 27. Water-vapour volume fraction in nozzle of Pelton injector for 820 m head with its (a) side view (b) front view and (c) Eroded nozzle of Chenani HPP.¹⁵

combinations of nozzle-needle angle, bend angle of nozzle pipe, as well as number and orientation of needle guide vanes.

Conclusions

The hydro-abrasive erosion in the Pelton turbine injector components, i.e. needle and nozzle has been analysed for various sediment parameters in addition to a range of design heads and nozzle opening conditions in this study. Further, the cavitation-prone region has also been identified and the effect of the HPP heads on the possibility of the occurrence of cavitation is also analysed. The major findings of this numerical study are summarized below.

- The size of the sediment has different effects on the nozzle and needle of the Pelton injector. As the size of sediment particles increases from 40 μm to 200 μm , the erosion rate of the nozzle increases by two times; however, the erosion rate of the needle reduces by 0.957 times. This has been mainly because of the dependence of the path of sediment particles in fluid on its inertia.
- With an increase in sediment concentration from 750 ppm to 3000 ppm, the erosion rate in both the nozzle and the needle increases by three times indicating a linear increment.
- With an increase in nozzle opening, minimal change has been observed in the erosion rate of the nozzle; however, the erosion rate of the needle has been found to vary quite significantly. The erosion rate has been found to decrease by 78.1% with an increase in stroke ratio from 0.35 to 0.8.
- The needle neck is susceptible to erosion due to sediments with high inertia which are also responsible for the formation of an erosion ring near the convergent region of the nozzle; whereas, erosion a little upstream of the needle tip is due to sediment with less inertia.
- Though the erosion rate of both the nozzle and needle has increased with the increment of the head from 200 m to 820 m, the rate of erosion in the nozzle and needle increased by 4.46 and 1.4 times, respectively. Likewise, the possibility of the occurrence of cavitation is more at the higher head especially above 600 m designed head. Consequently, the Pelton injector of a higher head HPP is more susceptible to the synergic effect of cavitation and hydro-abrasive erosion. The major region susceptible to cavitation has been found as the outlet of the nozzle near the nozzle ring.

Though the individual effects of cavitation and erosion have been captured in various components of the injector, this study is limited by the fact that the employed mathematical model fails to capture the material loss due to the combined effect of cavitation and hydro-abrasive erosion, which may result in enhanced injector wear. In the future, the effect of the eroded profile of the Pelton injector on the synergy effect of hydro-abrasive erosion and cavitation can be incorporated. Further, it is recommended

to optimize the Pelton injector for different hydro-abrasive erosion conditions.

Acknowledgements

The authors would like to thank Science and Engineering Research Board of India (Grant No. SRG/2020/002452), the National Natural Science Foundation of China (No. 50229088), the National Science and Technology Major Project of China (Y2019-I-0002-0003) and the Research Fund Program of State key Laboratory of Hydro-science and Engineering (sklhse-2022-KY-06, sklhse-2022-Iow13) for financially supporting the present work.

Declaration of conflicting interests

The author(s) declared no potential conflicts of interest with respect to the research, authorship, and/or publication of this article.

Funding

The author(s) disclosed receipt of the following financial support for the research, authorship, and/or publication of this article: This work was supported by the Research Fund Program of State key Laboratory of Hydrosience and Engineering (sklhse-2022-Iow13, sklhse-2022-KY-06), National Science and Technology Major Project of China (Y2019-I-0002-0003), Science and Engineering Research Board (SRG/2020/002452), and National Natural Science Foundation of China (50229088).

ORCID iDs

Navam Shrivastava  <https://orcid.org/0009-0000-0246-6515>

Anant Kumar Rai  <https://orcid.org/0000-0003-3675-5846>

Ali Abbas  <https://orcid.org/0000-0002-2474-0957>

Yexiang Xiao  <https://orcid.org/0000-0002-8864-4067>

References

1. IEA. *World energy outlook*. Paris: IEA- International Energy Agency, 2022. <https://www.iea.org/reports/world-energy-outlook-2022> accessed 15 May 2023
2. Shrivastava N and Rai AK. Assessment of sediment hazard and associated measurement. In: Pandey M, Azamathulla H and Pu JH (eds) *River dynamics and flood hazards: studies on risk and mitigation*. Singapore: Springer Nature Singapore, 2022, pp. 17–42. doi:10.1007/978-981-19-7100-6_2
3. Ang TZ, Salem M, Kamarol M, et al. A comprehensive study of renewable energy sources: classifications, challenges and suggestions. *Energy Strategy Rev.* 2022; 43: 100939. doi:10.1016/j.esr.2022.100939
4. Shah HA, Chaudhari GC, Dhiman VD, et al. A review on erosion of a Pelton turbine bucket. *J Phys Conf.* 2020; 1706: 012194. doi:10.1088/1742-6596/1706/1/012194
5. Sangal S, Singhal MK and Saini RP. Hydro-abrasive erosion in hydro turbines: a review. *Int J Green Energy.* 2018; 15(4): 232–253. doi:10.1080/15435075.2018.1431546
6. Padhy MK and Saini RP. A review on silt erosion in hydro turbines. *Renew Sustain Energy Rev.* 2008; 12(7): 1974–1987. doi:10.1016/j.rser.2007.01.025
7. Padhy MK and Saini RP. Study of silt erosion on performance of a Pelton turbine. *Energy.* 2011; 36: 141–147. doi:10.1016/j.energy.2010.10.060

8. Rai AK, Kumar A, Yexiang X, et al. Analysis and visualization of progressive erosion in Pelton buckets. *IOP Conf Ser Earth Environ Sci.* 2021; 774: 012105. doi:[10.1088/1755-1315/774/1/012105](https://doi.org/10.1088/1755-1315/774/1/012105)
9. Din MZU and Harmain GA. Assessment of erosive wear of Pelton turbine injector: nozzle and spear combination—a study of Chenani hydro-power plant. *Eng Fail Anal.* 2020; 116: 104695. doi:[10.1016/j.engfailanal.2020.104695](https://doi.org/10.1016/j.engfailanal.2020.104695)
10. Felix D, Abgottspon A, von Burg M, et al. Hydro-abrasive erosion on coated Pelton turbines: nine years of measurements and temporary shutdowns of HPP Fieschertal. In: 13th International Conference on Hydraulic Efficiency Measurement, Grenoble, France, 03–05 October 2022. DOI: [10.3929/ethz-b-000575182](https://doi.org/10.3929/ethz-b-000575182).
11. Alomar OR, Abd HM, Salih MM, et al. Performance analysis of Pelton turbine under different operating conditions: an experimental study. *Ain Shams Eng J.* 2022; 13(4): 101684. doi:[10.1016/j.asej.2021.101684](https://doi.org/10.1016/j.asej.2021.101684)
12. Rai AK and Kumar A. Continuous measurement of suspended sediment concentration: technological advancement and future outlook. *Measurement.* 2015; 76: 209–227. doi:[10.1016/j.measurement.2015.08.013](https://doi.org/10.1016/j.measurement.2015.08.013)
13. Kumar M, Kumar A and Saini RP. CFD analysis of silt erosion in pelton turbine. *Int Res J Commerce Arts Sci* 2015; 7(2): 110–119.
14. Ge X, Sun J, Chu D, et al. Sediment erosion on pelton turbines: a review. *Chin J Mech Eng.* 2023; 36(1): 1–27. doi:[10.1186/s10033-023-00880-y](https://doi.org/10.1186/s10033-023-00880-y)
15. Padhy MK and Saini RP. Effect of size and concentration of silt particles on erosion of Pelton turbine buckets. *Energy.* 2009; 34(10): 1477–1483. doi:[10.1016/j.energy.2009.06.015](https://doi.org/10.1016/j.energy.2009.06.015)
16. Rai AK, Kumar A and Staubli T. Effect of concentration and size of sediments on hydro-abrasive erosion of Pelton turbine. *Renew Energy.* 2020; 145: 893–902. doi:[10.1016/j.renene.2019.06.012](https://doi.org/10.1016/j.renene.2019.06.012)
17. Kumar K, Saini G, Kumar A, et al. Effective monitoring of Pelton turbine based hydropower plants using data-driven approach. *Int J Electr Power Energy Syst.* 2023; 149: 109047. doi:[10.1016/j.ijepes.2023.109047](https://doi.org/10.1016/j.ijepes.2023.109047)
18. Rai AK, Kumar A and Staubli T. Hydro-abrasive erosion in Pelton buckets: classification and field study. *Wear.* 2017; 392: 8–20. doi:[10.1016/j.wear.2017.08.016](https://doi.org/10.1016/j.wear.2017.08.016)
19. Bajracharya TR, Acharya B, Joshi CB, et al. Sand erosion of Pelton turbine nozzles and buckets: a case study of Chilime Hydropower Plant. *Wear.* 2008; 264(3–4): 177–184. doi:[10.1016/j.wear.2007.02.021](https://doi.org/10.1016/j.wear.2007.02.021)
20. Abgottspon A, Staubli T and Felix D. Erosion of Pelton buckets and changes in turbine efficiency measured in the HPP Fieschertal. *IOP Conf Ser Earth Environ Sci.* 2016; 49(12): 122008. doi:[10.1088/1755-1315/49/12/122008](https://doi.org/10.1088/1755-1315/49/12/122008)
21. Felix D, Albayrak I, Abgottspon A, et al. Hydro-abrasive erosion of hydraulic turbines caused by sediment—a century of research and development. *IOP Conf Ser Earth Environ Sci.* 2016; 49(12): 122001. doi:[10.1088/1755-1315/49/12/122001](https://doi.org/10.1088/1755-1315/49/12/122001)
22. Felix D. *Experimental investigation on suspended sediment, hydro-abrasive erosion and efficiency reductions of coated Pelton turbines.* PhD Thesis. Switzerland: ETH Zurich, 2017. Diss. 24145.
23. Rai AK, Kumar A and Staubli T. Financial analysis for optimization of hydropower plants regarding hydro-abrasive erosion: a study from Indian Himalayas. *IOP Conf Ser Earth Environ Sci* 2019; 240(2): 022025. doi:[10.1088/1755-1315/240/2/022025](https://doi.org/10.1088/1755-1315/240/2/022025)
24. Lee FZ, Lai JS and Sumi T. Reservoir sediment management and downstream river impacts for sustainable water resources—case study of shihmen reservoir. *Water.* 2022; 14(3): 479. doi:[10.3390/w14030479](https://doi.org/10.3390/w14030479)
25. Tarodiya R, Khullar S and Levy A. Assessment of erosive wear performance of Pelton turbine injectors using CFD-DEM simulations. *Powder Technol.* 2022; 408: 117763. doi:[10.1016/j.powtec.2022.117763](https://doi.org/10.1016/j.powtec.2022.117763)
26. Arora N, Kumar A and Singal SK. Technological advancement in measurements of suspended sediment and hydraulic turbine erosion. *Measurement.* 2022; 190: 110700. doi:[10.1016/j.measurement.2022.110700](https://doi.org/10.1016/j.measurement.2022.110700)
27. Leguizamón S, Jahanbakhsh E, Alimirzazadeh S, et al. Multiscale simulation of the hydroabrasive erosion of a Pelton bucket: bridging scales to improve the accuracy. *Int J Turbomach Propul Power.* 2019; 4(2): 9. doi:[10.3390/ijtp4020009](https://doi.org/10.3390/ijtp4020009)
28. Guo B, Xiao Y, Rai AK, et al. Sediment-laden flow and erosion modeling in a Pelton turbine injector. *Renew Energy.* 2020; 162: 30–42. doi:[10.1016/j.renene.2020.08.032](https://doi.org/10.1016/j.renene.2020.08.032)
29. Din MZU and Harmain GA. An assessment of sediment erosion of Pelton buckets using CFD. *Int J Hydropower Dams* 2021; 28(5): 85–89.
30. Bajracharya TR, Shrestha R, Sapkota A, et al. Modelling of hydroabrasive erosion in pelton turbine injector. *Int J Rotating Mach.* 2022; 2022: 1–15. doi:[10.1155/2022/9772362](https://doi.org/10.1155/2022/9772362)
31. Chongji Z, Yexiang X, Wei Z, et al. Pelton turbine needle erosion prediction based on 3D three-phase flow simulation. *IOP Conf Ser Earth Environ Sci.* 2014; 22(5): 052019. doi:[10.1088/1755-1315/22/5/052019](https://doi.org/10.1088/1755-1315/22/5/052019)
32. Staubli T, Abgottspon A, Weibel P, et al. Jet quality and Pelton efficiency. In: Proceeding of Hydro-2009, Lyon, France, 26-28 October 2009.
33. Jo IC, Park JH, Kim JW, et al. Jet quality characteristics according to nozzle shape of energy-recovery Pelton turbines in pressure-retarded osmosis. *Desalination Water Treat.* 2016; 57(51): 24626–24635. doi:[10.1080/19443994.2016.1152641](https://doi.org/10.1080/19443994.2016.1152641)
34. Messa GV, Mandelli S and Malavasi S. Hydro-abrasive erosion in Pelton turbine injectors: a numerical study. *Renew Energy.* 2019; 130: 474–488. doi:[10.1016/j.renene.2018.06.064](https://doi.org/10.1016/j.renene.2018.06.064)
35. Tarodiya R, Khullar S and Levy A. Particulate flow and erosion modeling of a Pelton turbine injector using CFD-DEM simulations. *Powder Technol.* 2022; 399: 117168. doi:[10.1016/j.powtec.2022.117168](https://doi.org/10.1016/j.powtec.2022.117168)
36. Liu J, Pang J, Liu X, et al. Analysis of sediment and water flow and erosion characteristics of large pelton turbine injector. *Processes.* 2023; 11(4): 1011. doi:[10.3390/pr11041011](https://doi.org/10.3390/pr11041011)
37. Bajracharya TR, Shrestha R and Timilsina AB. Numerical modelling of the sand particle flow in pelton turbine injector. *J Eng Issues Solut.* 2021; 1: 88–105. doi:[10.3126/joeis.v1i1.36821](https://doi.org/10.3126/joeis.v1i1.36821)
38. Han L, Duan XL, Gong RZ, et al. Physic of secondary flow phenomenon in distributor and bifurcation pipe of Pelton turbine. *Renew Energy* 2019; 131: 159–167.
39. Zhang Z and Casey M. Experimental studies of the jet of a Pelton turbine. *Proc Inst Mech Eng A J Power Energy* 2007; 221(8): 1181–1192. DOI: [10.1243/09576509JPE4](https://doi.org/10.1243/09576509JPE4).
40. Rossetti A, Pavesi G, Ardizzon G, et al. Numerical analyses of cavitating flow in a Pelton turbine. *J Fluid Eng.* 2014; 136(8): 081304. doi:[10.1115/1.4027139](https://doi.org/10.1115/1.4027139)

41. Zeng CJ, Xiao YX, Zhu W, et al. Numerical simulation of cavitation flow characteristic on Pelton turbine bucket surface. *IOP Conf Ser Mater Sci Eng*. 2015; 72: 042043. doi:[10.1088/1757-899X/72/4/042043](https://doi.org/10.1088/1757-899X/72/4/042043)
42. Gohil PP and Saini RP. Coalesced effect of cavitation and silt erosion in hydro turbines—a review. *Renew Sustain Energy Rev*. 2014; 33: 280–289. doi:[10.1016/j.rser.2014.01.075](https://doi.org/10.1016/j.rser.2014.01.075)
43. Thapa B, Chaudhary P, Dahlhaug OG, et al. Study of combined effect of sand erosion and cavitation in hydraulic turbines. In: International conference on small hydropower - Hydro Kandy. *Sri Lanka*. October 2007; 22.
44. Guo B, Li YH, Xiao YX, et al. Numerical analysis of sand erosion for a pelton turbine injector at high concentration. *IOP Conf Ser Earth Environ Sci*. 2021; 627: 012022. doi:[10.1088/1755-1315/627/1/012022](https://doi.org/10.1088/1755-1315/627/1/012022)
45. ANSYS. *Fluent theory guide 15.0*. USA: ANSYS, Inc., 2013.
46. Oka YI, Ohnogi H, Hosokawa T, et al. The impact angle dependence of erosion damage caused by solid particle impact. *Wear*. 1997; 203: 573–579. doi:[10.1016/S0043-1648\(96\)07430-3](https://doi.org/10.1016/S0043-1648(96)07430-3)
47. Oka YI, Okamura K and Yoshida T. Practical estimation of erosion damage caused by solid particle impact: Part 1: effects of impact parameters on a predictive equation. *Wear*. 2005; 259(1–6): 95–101. doi:[10.1016/j.wear.2005.01.039](https://doi.org/10.1016/j.wear.2005.01.039)
48. Oka YI, Matsumura M and Kawabata T. Relationship between surface hardness and erosion damage caused by solid particle impact. *Wear*. 1993; 162: 688–695. doi:[10.1016/0043-1648\(93\)90067-V](https://doi.org/10.1016/0043-1648(93)90067-V)
49. Oka YI and Yoshida T. Practical estimation of erosion damage caused by solid particle impact: Part 2: mechanical properties of materials directly associated with erosion damage. *Wear*. 2005; 259(1–6): 102–109. doi:[10.1016/j.wear.2005.01.040](https://doi.org/10.1016/j.wear.2005.01.040)
50. Rosin P. The law governing the fineness of powdered coal. *J Inst Fuel* 1993; 7: 29–36.
51. Schnerr GH and Sauer J. Physical and numerical modeling of unsteady cavitation dynamics. In: Fourth international conference on multiphase flow. New Orleans, LO, USA: ICMF New Orleans, Vol. 1, 2001.
52. Benzon D, Zidonis A, Panagiotopoulos A, et al. Numerical investigation of the spear valve configuration on the performance of Pelton and Turgo turbine injectors and runners. *J Fluid Eng*. 2015; 137(11): 111201. doi:[10.1115/1.4030628](https://doi.org/10.1115/1.4030628)
53. Jeon H, Park JH, Shin Y, et al. Friction loss and energy recovery of a Pelton turbine for different spear positions. *Renew Energy*. 2018; 123: 273–280. doi:[10.1016/j.renene.2018.02.038](https://doi.org/10.1016/j.renene.2018.02.038)
54. Boes R. Real-time monitoring of suspended sediment concentration and particle size distribution in the headwater way of a high-head hydropower plant. In: Water engineering for sustainable environment: 33rd IAHR congress, Vancouver, BC, 9–14 August 2009, pp. 4037–4044.
55. IEC 62364. *Hydraulic machines – guidelines for dealing with hydro-abrasive erosion in Kaplan, Francis, and Pelton turbines*. Geneva, Switzerland: International Electrotechnical Commission, 2019.
56. Rai AK, Kumar A, Staubli T, et al. Interpretation and application of the hydro-abrasive erosion model from IEC 62364 (2013) for Pelton turbines. *Renew Energy*. 2020; 160: 396–408. doi:[10.1016/j.renene.2020.06.117](https://doi.org/10.1016/j.renene.2020.06.117)
57. Sharma A. *Investigation of sand erosion of Pelton turbine in Chenani hydro electric Project-I (5 x 4.66 MW)*. Master thesis. India: Indian Institution of Technology Roorkee, 2019.
58. Dular M, Stoffel B and Sirok B. Development of a cavitation erosion model. *Wear*. 2006; 261(5–6): 642–655. doi:[10.1016/j.wear.2006.01.020](https://doi.org/10.1016/j.wear.2006.01.020)
59. Hong S, Wu Y, Wu J, et al. Effect of flow velocity on cavitation erosion behavior of HVOF sprayed WC-10Ni and WC-20Cr3C2–7Ni coatings. *Int J Refract Metals Hard Mater*. 2020; 92: 105330. doi:[10.1016/j.jrmhm.2020.105330](https://doi.org/10.1016/j.jrmhm.2020.105330)
60. Shrivastava N and Rai AK. Parametric investigation of Pelton turbine injector under hydro-abrasive erosion conditions. *J Appl Fluid Mech* 2024; 17(1): 89–104. doi:[10.47176/JAFM.17.1.2126](https://doi.org/10.47176/JAFM.17.1.2126)